nature metabolism

Letter

https://doi.org/10.1038/s42255-025-01280-3

Rapid modulation of gut microbiota composition by hypothalamic circuits in mice

Received: 30 April 2024

Accepted: 17 March 2025

Published online: 22 April 2025

Check for updates

A list of authors and their affiliations appears at the end of the paper

In recent years, the gut microbiota and derived metabolites have emerged as relevant players in modulating several brain functions, including energy balance control[1–3]. This form of distant communication mirrors that of metabolic hormones (for example, leptin, ghrelin), which convey information about the organism's energy status by exerting effects on diverse brain regions, including the master homeostatic centre, the hypothalamus[4]. However, whether the hypothalamus is also able to influence gut microbiota composition remains enigmatic. Here we present a study designed to unravel this challenging question. To this aim, we used chemogenetics[5] (to selectively activate or inhibit hypothalamic pro-opiomelanocortin or agouti-related peptide neurons) or centrally administered leptin or ghrelin to male mice. Subsequently, we conducted microbiota composition analysis throughout the gut using 16S rRNA gene sequencing. Our results showed that these brain interventions significantly changed the gut microbiota in an anatomical and short-term (2–4 h) fashion. Transcriptomic analysis indicated that these changes were associated with the reconfiguration of neuronal and synaptic pathways in the duodenum concomitant with increased sympathetic tone. Interestingly, diet-induced obesity attenuated the brain-mediated changes triggered by leptin in gut microbiota communities and sympathetic activation. Our findings reveal a previously unanticipated brain–gut axis that acutely attunes microbiota composition on fast timescales, with potential implications for meal-to-meal adjustments and systemic energy balance control.

Over the last two decades, many studies have shown that changing the gut microbiota composition has the potential to positively influence the progression of several diseases[1]. Therefore, the gut microbiota is emerging as a crucial determinant for the maintenance and promotion of host homeostasis and health[1]. This bacterial ecosystem is a complex and dynamic entity that produces many active compounds that are involved in a wide range of organismal functions. In the context of energy balance, the availability and abundance of different bacterial-derived metabolites (for example, short-chain fatty acids, bile acid derivatives, endocannabinoids) may profoundly influence host metabolism and feeding behaviour via diverse brain mechanisms[1,2,6]. Indeed, the interaction of these metabolites with G protein-coupled receptors of enteroendocrine cells promotes indirect signalling to the brain through the release of gut hormones (glucagon-like peptide-1, peptide YY) and neurotransmitters (γ-aminobutyric acid, serotonin)[1]. Furthermore, growing evidence suggests that many bacterial-derived metabolites reach the bloodstream and exert direct effects on distal organs, including the brain[7]. Collectively, these data indicate that

A full list of affiliations appears at the end of the paper. e-mail: patrice.cani@uclouvain.be; ruben.nogueiras@usc.es; mclaret@recerca.clinic.cat

https://doi.org/10.1038/s42255-025-01280-3

certain metabolites produced by intestinal bacterial communities contribute to fine-tuning inflammation, glucose and lipid metabolism, and appetite via the so-called microbiota–gut–brain axis[3].

This mode of communication used by the gut microbiota mirrors the strategies used by metabolic organs (stomach, white adipose tissue or pancreatic beta cells, among others), which secrete hormones (ghrelin, leptin and insulin, respectively) that signal the whole-body energy status to the brain[4]. In turn, the brain integrates this information and orchestrates a range of adaptive mechanisms. For example, pro-opiomelanocortin (POMC) and agouti-related peptide (AgRP) neurons located in the arcuate nucleus (ARC) of the hypothalamus can sense and amalgamate multiple dynamic cues conveyed by metabolic hormones (ghrelin, leptin), nutrients and sensory inputs[4]. According to this information, these neurons co-ordinately modulate appetite, energy expenditure and glucose and lipid metabolism via the autonomic regulation of peripheral tissues, thus adjusting overall energy balance and metabolism[4]. On this basis, the brain also communicates with the gut and regulates key gastrointestinal functions (motility, permeability, pH, mucus production, immune response)[8]. However, whether the brain is also able to influence gut microbiota composition remains enigmatic.

This study was designed to unravel this challenging hypothesis. Our results unequivocally show that acute modulation of POMC or AgRP neuronal activity via chemogenetics, as well as the central delivery of the metabolic hormones ghrelin and leptin, changes gut microbiota composition in a short-term and anatomically specific fashion. Together, our findings reveal a new and unexpected brain–gut axis that acutely attunes microbiota composition on rapid timescales, with potential implications for meal–meal adjustments and systemic energy balance control. These observations represent a paradigm shift because they introduce the brain as an active modulator of microbiome plasticity and composition in response to metabolic signals.

To initially assess whether the brain influences gut microbiota composition, we chemogenetically modulated the activity of hypothalamic AgRP and POMC neurons. These populations of neurons are plausible candidates to mediate brain–gut communication because of their crucial role in systemic metabolic control[4]. To this aim, we used designer receptors exclusively activated by designer drugs (DREADD) technology[5]. *AgRP*$^{Cre/+9}$ or *POMC*$^{Cre/+10}$ mice, as well as *AgRP*$^{+/+}$ or *POMC*$^{+/+}$ as controls, were bilaterally injected with an adeno-associated virus (AAV) vector encoding excitatory hM3Dq (AAV8-hSYN-DIO-hM3D(Gq)-mCherry) or inhibitory hM4Di (AAV8-hSYN-DIO-hM4D(Gi)-mCherry) DREADDs in the ARC (Fig. 1a). Subsequent studies were conducted 3 weeks later to ensure adequate AAV expression. Validation of the fidelity of AAV infection and the effectiveness of DREADD performance on AgRP and POMC neurons was confirmed via immunofluorescence studies (Extended Data Fig. 1a–h).

The DREADD ligand clozapine *N*-oxide (CNO) was administered to selectively activate or inhibit POMC or AgRP neurons; gut luminal contents from four anatomically distinct segments (duodenum, jejunum, ileum and caecum) were collected 2 and 4 h later, followed by gut microbiota analysis (Fig. 1a). To assess how the composition of microbial communities changed upon brain manipulations, we implemented a tailored metagenomic profiling and statistical analysis pipeline (Fig. 1b). Microbiota community richness and evenness was evaluated according to the α-diversity using the Shannon index. We observed that modulation of the activity of AgRP or POMC neurons did not significantly modify this parameter (Fig. 1c–f). Beta diversity analysis was performed to obtain the differential abundant taxa using the analysis of compositions of microbiomes with bias correction (ANCOM-BC) method[11]. Stimulation of AgRP neurons resulted in minor changes in the bacterial profile (Fig. 1g), while inhibition also induced slight changes in the gut microbiota composition of the jejunum and caecum (Fig. 1g). In contrast, activation of POMC neurons predominantly increased or decreased several bacterial families in the duodenum, while inhibition significantly affected bacterial families in the jejunum, ileum and caecum (Fig. 1g). These changes in microbiome composition were not due to alterations in gut motility (Extended Data Fig. 2a–e). Collectively, our findings suggest that the acute chemogenetic manipulation of key populations of hypothalamic neurons (particularly POMC neurons) results in rapid changes in gut microbiota composition independent of food intake.

To investigate these findings under a more physiological context, we implemented two complementary strategies that progressed with the modulation of hypothalamic AgRP and POMC neurons: (1) sensory perception of food[12–15] and (2) central administration of metabolic hormones (that is, ghrelin and leptin)[4,12,16]. Regarding the sensory aspect, overnight fasted C57BL/6J mice were exposed either to a caged inedible object (a wood dowel) or a caged food pellet that could be seen and smelled but not consumed (Fig. 2a). Mice were euthanized at a shorter time interval (1 h later), compatible with the acute food sensory effects on hypothalamic neurons[12–15]; luminal contents were obtained from the diverse gut regions for microbiota analysis. The diversity of the microbial communities was similar between experimental groups (Fig. 2b). Similarly, sensory detection of food did not cause changes in gut microbiota composition in any of the intestinal segments assessed (Fig. 2c). These results indicate that transient fluctuations in AgRP and POMC neuron activity in response to food perception are insufficient to influence the gut microbiome, suggesting that more sustained or intense stimuli may be required to induce noticeable changes. Nevertheless, we cannot exclude that the timing of sample collection could be contributing to the absence of changes in microbiota composition under these experimental conditions.

Next, we examined the effects of ghrelin and leptin, which are canonical metabolic hormones with opposite functions regarding

Fig. 1 | Activity modulation of AgRP and POMC neurons influences gut microbiota composition. a, Diagram illustrating the approach to express the excitatory (hM3Dq) or inhibitory (hM4Di) DREADDs in AgRP and POMC neurons. **b**, Schematic representation of the data processing and analysis workflow. **c**,**d**, Microbial α-diversity (Shannon index) of gut microbiota from vehicle and AgRP neuron-activated mice and vehicle (**c**) and AgRP neuron-inhibited mice 2 or 4 h after CNO injection (**d**). Sample sizes in **c**: 2 h control $n = 7$ in the duodenum, jejunum and caecum, and $n = 6$ in the ileum; 2 h activated $n = 8$ in the duodenum, jejunum and ileum, and $n = 6$ in the caecum; 4 h control $n = 8$ in duodenum and jejunum, and $n = 7$ in the ileum and $n = 6$ in the caecum; 4 h activated $n = 8$ in the duodenum, jejunum, ileum and caecum. Sample sizes in **d**: 2 h control $n = 7$ per gut section; 2 h inhibited $n = 9$ per gut section; 4 h control $n = 7$ per gut section; 4 h inhibited $n = 8$ in the duodenum, jejunum and ileum, and $n = 7$ in the caecum. **e**,**f**, Microbial α-diversity (Shannon index) of gut microbiota from vehicle and POMC neuron-activated mice (**e**) and vehicle and POMC neuron-inhibited mice (**f**) 2 or 4 h after CNO injection. Sample sizes in **e**: 2 h control $n = 7$ per gut section; 2 h activated $n = 8$ per gut section; 4 h control $n = 8$ per gut section; 4 h activated $n = 8$ per gut section. Sample sizes in **f**: 2 h control $n = 7$ in the duodenum, jejunum and ileum, and $n = 6$ in the caecum; 2 h inhibited $n = 9$ per gut section; 4 h control $n = 7$ per gut section; 4 h inhibited $n = 7$ in the duodenum, jejunum and ileum, and $n = 6$ in the caecum. *$q = 0.0212$. All box plots display the range from the first to the third quartile (box) and the median (centre line), while the whiskers extend to the minimum and maximum values. Statistical significance was determined using a one-way analysis of variance (ANOVA), followed by false discovery rate (FDR) adjustment. **g**, Heatmap representations from the ANCOM-BC analysis at the family level. Data are represented by the effect size (log fold change). Microbial taxa with statistically significant differences between the control and treated group at 2 and 4 h after CNO injection in specific gut sections are shown. Stars indicate statistically significant differences compared to the control group; *q* values for the differences depicted in the heatmaps are provided in Supplementary Table 1.

https://doi.org/10.1038/s42255-025-01280-3

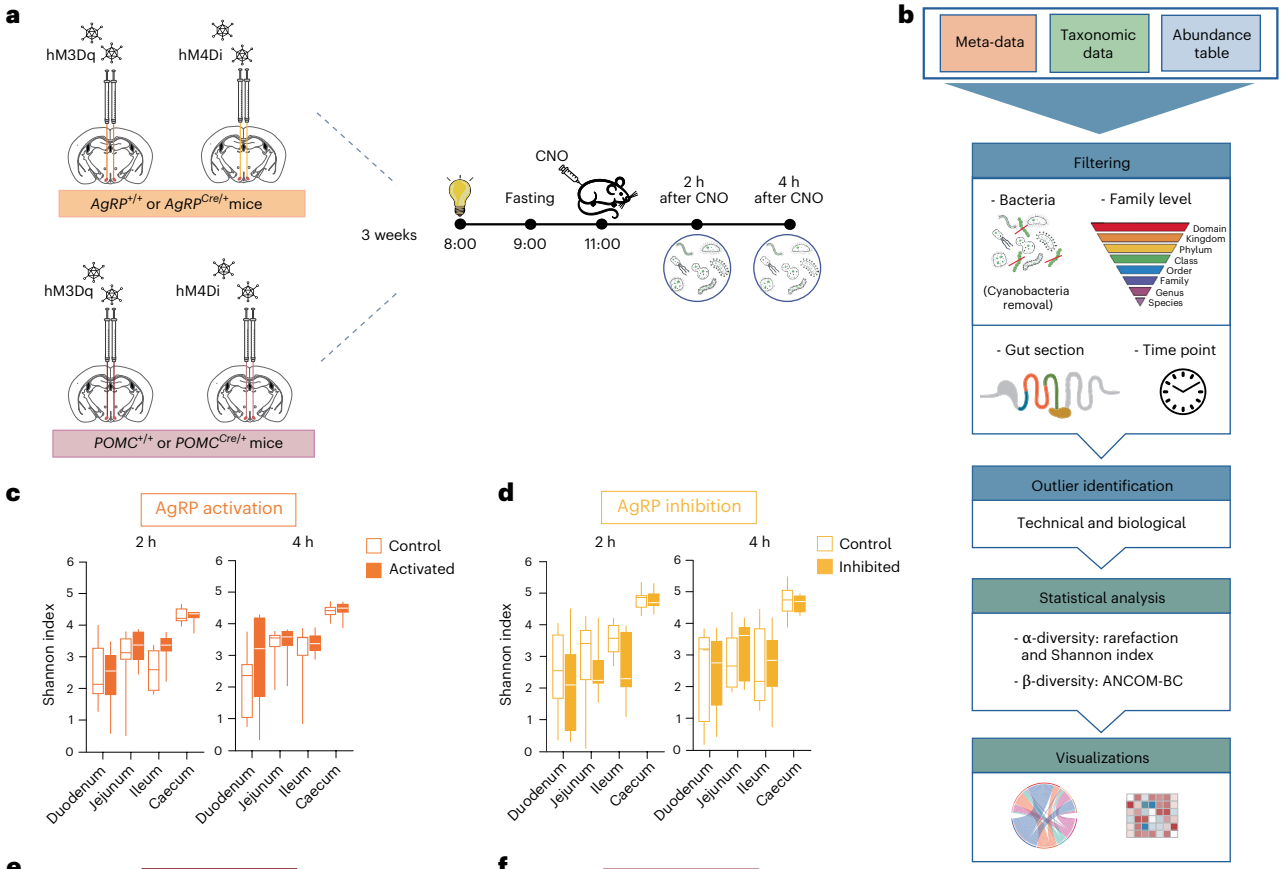

https://doi.org/10.1038/s42255-025-01280-3

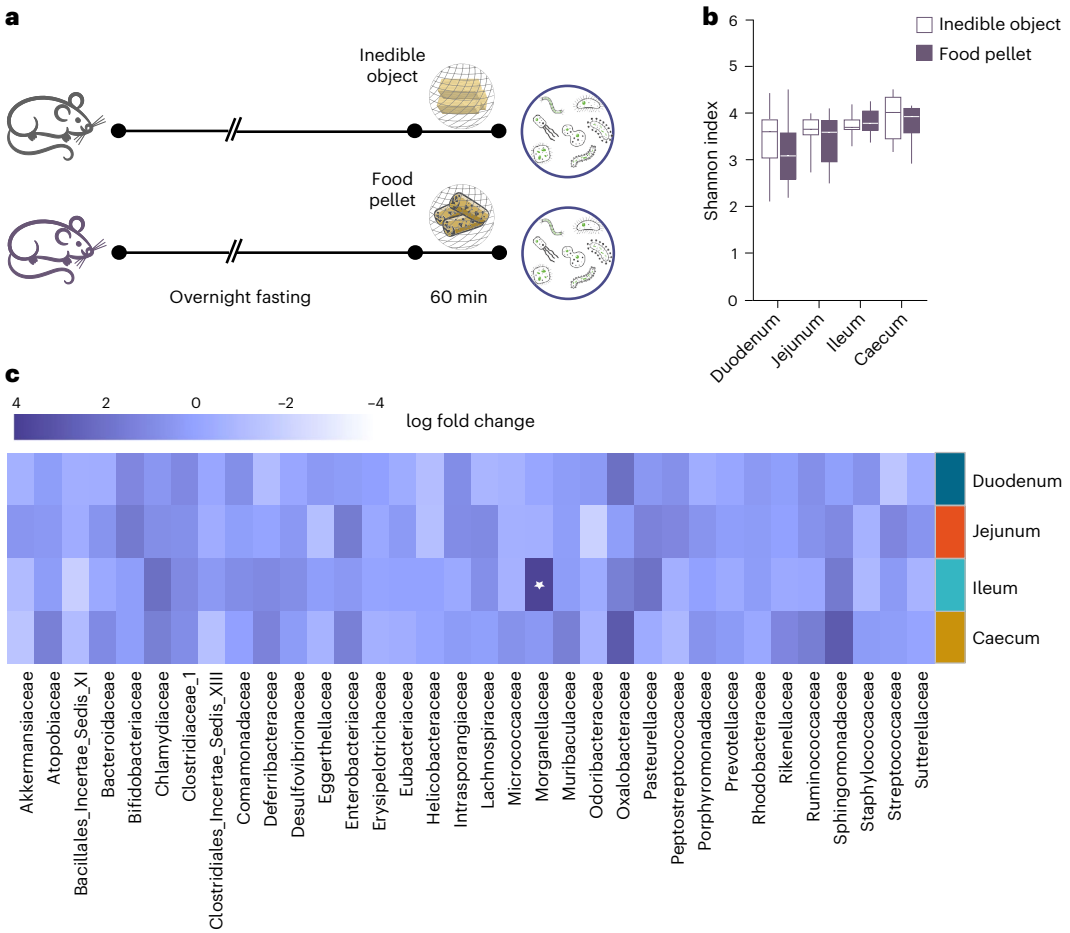

Fig. 2 | Sensory perception of food does not shape gut microbiota composition. a, Schematic representation of the food sensory perception paradigm. **b**, Microbial α-diversity (Shannon index) of gut microbiota from mice exposed to an inedible object ($n = 6$ samples per gut section) or inaccessible food pellet for 60 min ($n = 7$ samples per gut section). The box plot displays the range from the first to the third quartile (box) and the median (centre line), while the whiskers extend to the minimum and maximum values. Statistical significance was determined using a one-way ANOVA, followed by FDR adjustment. **c**, Heatmap representation from the ANCOM-BC analysis at the family level. Data are represented according to the effect size (log fold change). Stars indicate microbial taxa with statistically significant differences (*$q = 0.0144$) between an inedible object and an inaccessible food pellet after 60 min of exposure.

energy homeostasis[16]. To do so, we administered saline, leptin or ghrelin into the lateral ventricle of the brain of 8-week-old C57BL/6J mice (Fig. 3a). Validation of hormonal interventions was confirmed via FOS staining in hypothalamic sections (Extended Data Fig. 3a,b). Luminal contents from the duodenum, jejunum, ileum and caecum were collected 2 and 4 h after the injection (Fig. 3a). While ghrelin-associated α-diversity showed no significant differences between groups, leptin treatment led to significant changes in this parameter in certain gut regions (Fig. 3b,c). For β-diversity, similar to AgRP neuronal activation, ghrelin resulted in modest alterations in bacterial families (Fig. 3d). In contrast, leptin treatment led to notable variations in the composition of the microbiota across the various intestinal sections analysed. Indeed, changes were primarily observed in the ileum and caecum after 2 h of treatment, whereas the main changes at 4 h were evident in the duodenum (Fig. 3d). The latter anatomical changes were reminiscent of the effects seen after POMC neuronal activation. Interestingly, while ghrelin did not significantly affect gut motility, central leptin administration strongly inhibited this parameter (Extended Data Fig. 4a–e). Altogether, these results suggest that satiety signals contribute to reshaping the bacterial composition of the gut in a swift and anatomically selective manner. In the case of leptin, part of these changes may be the consequence of alterations in gut transit. This aligns with previous studies showing that leptin influences gastrointestinal motility[17], which can in turn affect microbial communities and dynamics in the gut.

For a comprehensive overview and precise identification of interactions between diverse treatments and gut sections, we visualized differentially abundant taxa using a chord diagram (Fig. 3e). This analysis revealed that the most significant brain-induced effects on gut microbiota composition were observed in the duodenum and were mediated by both chemogenetic POMC neuron activation and central leptin (Fig. 3e). Therefore, we subsequently focused our attention on this specific gut segment and hormonal treatment.

Central leptin resistance is a hallmark of obesity[16]. To assess whether leptin resistance compromises the leptin-driven changes in the gut microbiota profile, we fed C57BL/6J mice with a high-fat diet (HFD) for 12 consecutive weeks (Fig. 4a). As expected, this dietary regime caused significant weight gain, hyperglycaemia and plasma hyperleptinaemia (Extended Data Fig. 5a–c) indicative of leptin resistance. Notably, central leptin delivery in these animals (Fig. 4a) did not trigger the microbiota changes previously observed across the intestine of lean mice (Fig. 4b). No changes in α-diversity were observed (Extended Data Fig. 5d). Collectively, these results indicate that functional leptin signalling in the brain is required to drive short-term gut microbiota changes.

Changes in microbiota communities entail alterations in metabolic pathways and the production of metabolites that impact host health[3]. To define the metabolic and functional signatures of the microbial communities in the duodenum induced by central leptin administration,

https://doi.org/10.1038/s42255-025-01280-3

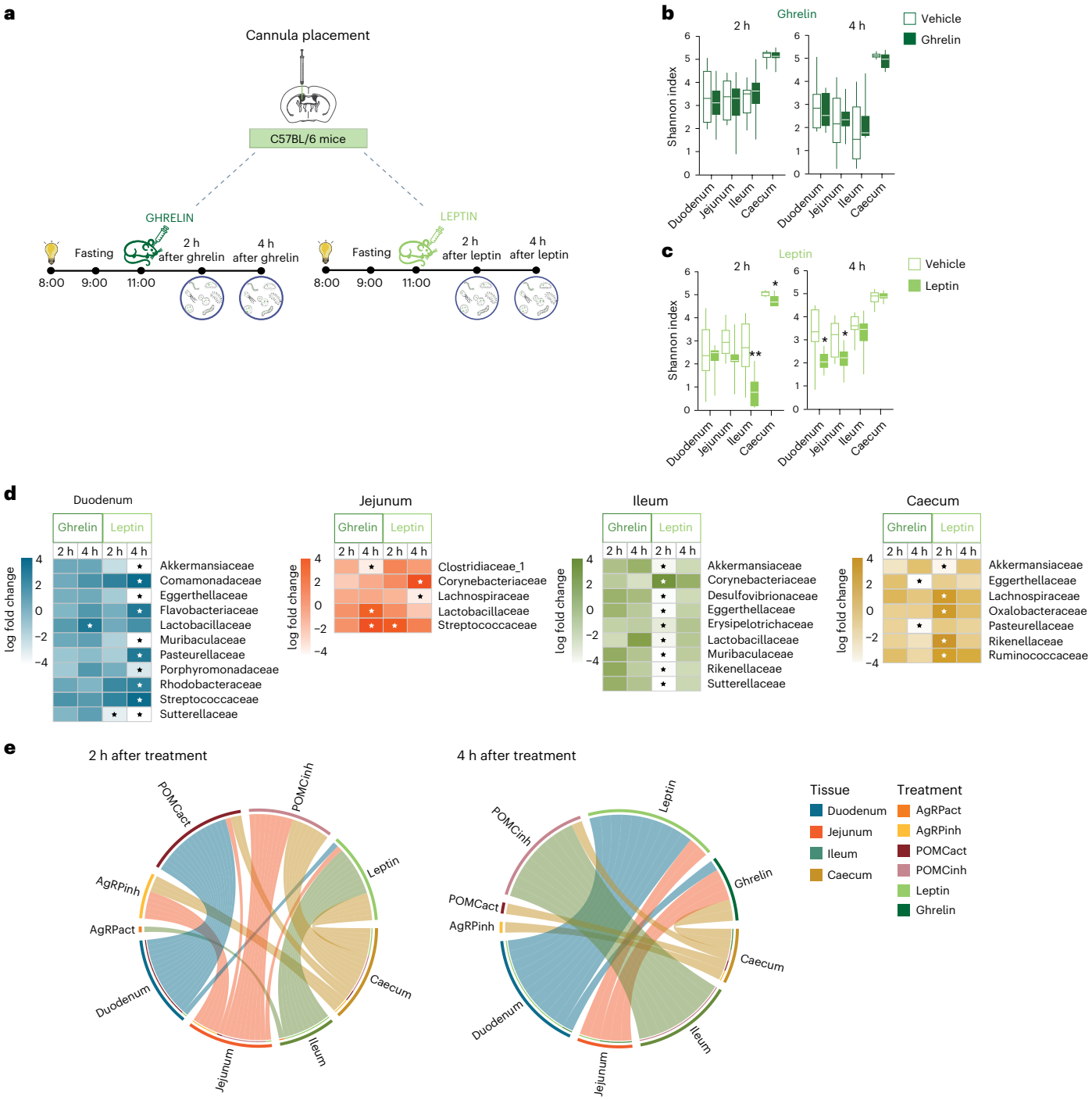

Fig. 3 | Central ghrelin or leptin administration causes rapid changes in gut microbiota composition. a, Schematic representation of the experimental outline for brain delivery of leptin and ghrelin. **b**,**c**, Microbial α-diversity (Shannon index) of gut microbiota from mice treated with ICV ghrelin (**b**) or leptin (**c**) at 2 or 4 h after treatment. Sample sizes in **b**: 2 h vehicle $n = 9$ per gut section; 2 h ghrelin $n = 10$ per gut section; 4 h vehicle and ghrelin $n = 10$ per gut section. Sample sizes in **c**: 2 h vehicle $n = 8$ per gut section; 2 h leptin $n = 7$ in the duodenum, jejunum and caecum, and $n = 8$ in the ileum; 4 h vehicle and leptin $n = 8$ in the duodenum, jejunum and caecum, and $n = 7$ in the ileum; 2 h (ileum, $^{**}q = 0.0036$; caecum, $^{*}q = 0.0101$); 4 h (duodenum, $^{*}q = 0.0152$; jejunum, $^{*}q = 0.0269$). All box plots display the range from the first to the third quartile (box) and the median (centre line), while the whiskers extend to the minimum and maximum values. Statistical significance was determined using a one-way ANOVA, followed by FDR adjustment. **d**, Heatmap representations from the ANCOM-BC analysis at the family level. Microbial taxa with statistically significant differences between control and treated group at 2 and 4 h after treatment in specific gut sections are shown. Data are represented by the effect size (log fold change). Stars indicate statistically significantly differences compared to the control group; q values for the differences depicted in the heatmaps are provided in Supplementary Table 1. **e**, Chord diagram where the width of the links represents the strength of the interaction between the treatment and the gut section in which the microbial changes are observed. AgRPact, activation of AgRP neurons; AgRPinh, inhibition of AgRP neurons; POMCact, activation of POMC neurons; POMCinh, inhibition of POMC neurons.

we used predictive tools of metagenome functions based on 16S rRNA sequencing data[18,19]. This analysis revealed 472 metabolic pathways, among which 79 exhibited significant differences (Extended Data Fig. 6). Most pathways reflected an enrichment in biosynthetic processes (amino acids, cofactors, carriers, vitamins, carbohydrates, lipids, precursor metabolites and energy) with few representations of degradative categories (Extended Data Fig. 6). It is important to note that some of the biochemical products of these pathways (for example, certain amino acids, acetate) have been associated with central acute effects on appetite in rodents[20–23].

To validate these predictions, we performed liquid chromatography (LC)–tandem mass spectrometry (MS/MS) metabolomics on the duodenal content from mice centrally treated with vehicle or leptin. Vehicle and leptin samples formed distinct clusters (Extended Data Fig. 7a). We identified 89 metabolites, 19 of which were significantly altered between groups (Fig. 4c,d). Leptin treatment notably increased amino acids and related metabolites (Fig. 4d), partially validating functional predictions for amino acid metabolism (Extended Data Fig. 6). Additionally, metabolites such as pyridoxic acid, trigonelline, pantothenic acid and riboflavin (Fig. 4d) support microbial contributions to vitamin biosynthesis pathways predicted by Phylogenetic Investigation of Communities by Reconstruction of Unobserved States (PICRUSt2) plug-in (Extended Data Fig. 6).

We next evaluated the neuroactive potential of the gut microbiota, after central leptin intervention, by examining the presence of gut–brain modules (GBMs) involved in the synthesis or degradation of neuroactive compounds[24]. Our findings revealed that intracerebroventricular (ICV) leptin administration was associated with reduced representation of several GBMs, including those involved in neurotransmitter synthesis (for example, γ-aminobutyric acid and glutamate) and the production of neuroactive metabolites (for example, quinolinic acid, vitamin K_2 and *p*-cresol) (Extended Data Fig. 7b). While highly speculative, these results suggest that activation of the brain–gut–microbiota axis via ICV leptin administration may transiently attenuate the reciprocal communication from the microbiota to the brain.

In an attempt to unveil potential mechanisms mediating the rapid reconfiguration of gut microbiota composition after central leptin delivery, we conducted RNA sequencing (RNA-seq) analysis of the duodenum under this experimental condition. We also included an antibiotic treatment to isolate the effects of the microbiota on transcriptomic changes. We concentrated on the 2-h time point, assuming that potential transcriptomic changes in the duodenum should precede any alterations in microbiota if they are causally linked (Fig. 4e). To gain insights into the functional characteristics and biological implications of central leptin administration across all experimental groups, we conducted a Gene Ontology (GO) analysis of the transcriptomic dataset. This uncovered a significant enrichment of common pathways between the control (water) and antibiotic treatment groups after ICV leptin administration, including 'Neuronal signalling and synaptic processes', 'Cellular signalling, transport and ion regulation', 'Developmental and differentiation processes' and 'Hormonal regulation, blood circulation and metabolism' (Fig. 4f). Additionally, leptin administration enhanced pathways related to 'Immune response and antigen processing' in the antibiotic-treated group (Fig. 4f). These results indicate that central leptin delivery engages in neuronal communication processes in the duodenum independently of the gut microbiota, underscoring the establishment of dynamic brain–gut communication mechanisms.

The sympathetic nervous system (SNS) has a crucial role in regulating diverse metabolic functions that are essential for maintaining energy balance and physiological homeostasis[25]. In particular, the melanocortin system and leptin signalling influence the function of several peripheral tissues via the SNS[26,27]. Sympathetic neurons signal, via catecholamines (mainly adrenaline and noradrenaline), to α-adrenergic or β-adrenergic receptors in target cells. In this context, we next set out to determine whether central leptin modulates the duodenal content of adrenaline and noradrenaline. We found that while leptin did not change the concentration of noradrenaline in the duodenum 2 h after administration, it increased adrenaline levels (Fig. 4g,h), suggesting increased duodenal sympathetic tone. This is congruent with the transcriptomic data, reflecting the recruitment of pathways related to neuronal signalling and synaptic transmission (Fig. 4f). Interestingly, mice fed with an HFD did not exhibit a rise in duodenal adrenaline induced by central leptin (Fig. 4g). These results suggest that intact leptin signalling is necessary to mediate brain–gut sympathetic communication. This aligns with the attenuated changes in microbiota composition previously observed under the HFD regime (Fig. 4b).

This study represents a new standpoint and a paradigm shift in microbiota biology and metabolic research for several reasons. First, we provide evidence that the direct action of metabolic hormones in the brain (for example, leptin) and modulation of key neurons implicated in energy balance control (for example, POMC neurons) result in acute and anatomically specific alterations in gut microbiota composition. Our findings uncover a new and unexpected layer of communication between the brain and the gut microbiota, with potential physiological significance (in managing the postprandial state) and pathophysiological relevance.

Second, our work builds on previous studies demonstrating rapid changes in gut microbiota composition induced by diurnal rhythmicity[28,29], dietary manipulations[30,31] and neurological insults, including stress[32–34]. Notably, our data extend these observations by offering gut-region-specific insights into gut microbiota composition that are independent of food intake and nutrient availability. Indeed, most of the current knowledge on gut microbiota biology stems from studies of faecal samples, which is an appropriate non-invasive strategy that can be sampled easily and repeatedly. However, the faecal microbiota composition provides a snapshot of the overall microbial diversity of the entire gastrointestinal tract. This approach precludes the analysis of regional variations and potential rapid changes (for example, 2 h) in microbiota composition, which is important to understand how microbial communities adapt to specific niches and their contribution to host

Fig. 4 | Leptin signalling is necessary to induce short-term alterations in the gut microbiota. a, Schematic representing the experimental outline of central leptin treatment under HFD conditions. **b**, Heatmap representations from the ANCOM-BC analysis at the family level. Data are represented by the effect size (log fold change). Microbial taxa with statistically significant differences between vehicle-treated and leptin-treated groups in mice fed with standard diet (SD) (left heatmap) and mice fed with an HFD (right heatmap) at 2 and 4 h after treatment in specific gut sections are shown (n = 7–10 mice per group). Stars indicate statistically significant differences compared to the control group; q values for the differences depicted in the heatmaps are provided in Supplementary Table 1. **c**, Volcano plot displaying statistically significant differences in metabolites in the duodenal luminal content between mice centrally treated with vehicle or leptin (red, upregulated; blue, downregulated; black, no changes; n = 6 mice per group). **d**, Bar plot visualization of significantly changed metabolites ($\log_2$ fold change). **e**, Schematic representing the experimental outline of the antibiotic and central leptin treatment study. **f**, Sankey plot of the top 50 overrepresented GO pathways and related biological categories for the leptin versus vehicle groups comparing untreated (water, left) or antibiotic-treated (right) conditions (n = 6–14 mice per group). The GO pathways are ordered according to ascending P value. Details on GO categories and P values are provided in Supplementary Table 2. **g**,**h**, Adrenaline (**g**) and noradrenaline (**h**) levels in the duodenum of mice fed with standard or HFD 2 h after central leptin treatment. Sample sizes in **g**: vehicle (n = 6); leptin, vehicle HFD and leptin HFD (n = 8). Sample sizes in **h**: n = 8 per group. **g**,**h**, Data are represented as the mean ± s.e.m. *P = 0.0313, ***P = 0.0006, ****P < 0.0001. Statistical significance was determined using a two-way ANOVA followed by Tukey's test.

https://doi.org/10.1038/s42255-025-01280-3

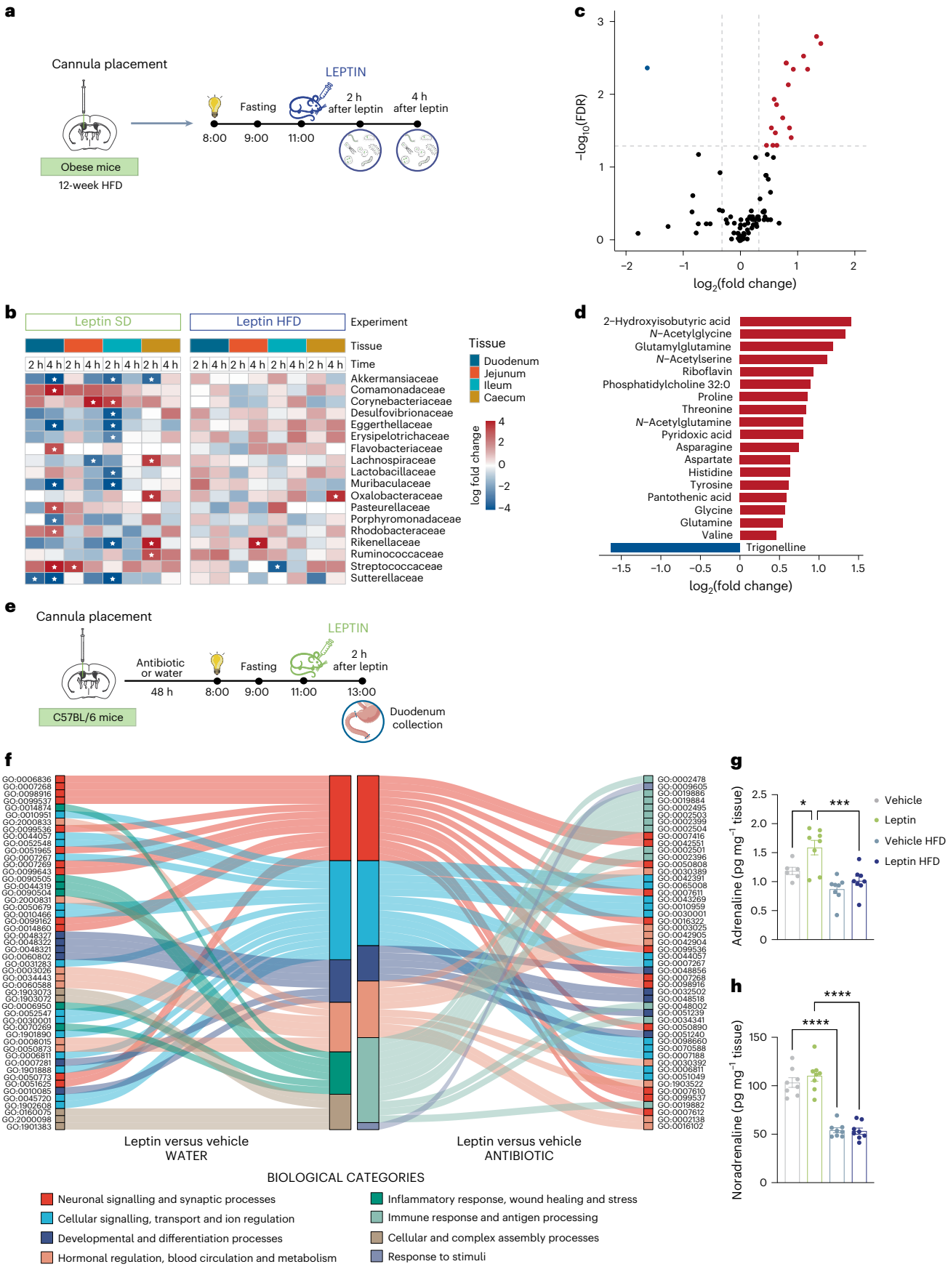

health. Considering that the small intestine serves as the primary site for nutrient digestion and absorption, it is reasonable to anticipate that nutrients can rapidly influence gut microbiota activity and composition in this gut segment. Our experimental design, centred around 2-h and 4-h intervals, reinforces this idea and emphasizes the importance of analysing specific regions and using short time points.

Third, our study also underscores the dynamic nature of the gut microbiome in response to immediate metabolic cues. Therefore, it is tempting to speculate that the rapid brain-mediated changes in gut microbiota may have a meal–meal relevance with a direct impact on systemic metabolism. While food intake is vital for the provision of energy and nutrients, it is also a significant stressor that disrupts homeostasis[35]. Indeed, these microbiome changes could contribute to multiple postprandial physiological aspects, including nutrient absorption, immune function, maintenance of the gastrointestinal barrier and integrity, and production of bioactive metabolites, as well as metabolism and appetite regulation. Our findings indicating that leptin-induced changes in bacterial functional pathways can be associated with changes in metabolites that acutely modulate appetite support this idea. The dynamic brain–gut reshaping of microbial communities could represent an evolutionary strategy to handle the postprandial situation and fine-tune appetite, thus maximizing metabolic benefits and reducing homeostatic stress.

Our transcriptomic data suggest that brain–gut communication occurs through the reorganization of the neuronal and synaptic architecture of the duodenum, independent of gut microbiota. In line with this, we also noted a local increase in sympathetic mediators indicating enhanced SNS activity. Notably, this effect was attenuated under HFD feeding, implying that obesogenic states may disrupt adequate brain–gut communication. Nevertheless, we cannot rule out the potential involvement of circulating factors (hormones, peptides) released by the brain that directly or indirectly mediate the communication between the brain and the gut. This would depict a complex scenario in which multiple factors could act in conjunction with neural pathways or independently to influence gut microbiota and function.

Despite this study providing a new dimension in the way that the brain communicates with the periphery, it is important to recognize some limitations. We used pharmacological interventions (that is, exogenous administration of hormones and DREADD ligand in line with those commonly used in the literature), aimed at eliciting robust responses. While our studies were consistently conducted at the same time during the light phase, we believe that the pharmacological treatments used would drive the same observed outcomes regardless of time of day. The dissection of the functional relevance and mechanistic insights of brain-mediated variations in gut microbiota are challenged by the inability to exclude confounding factors or define appropriate biological readouts. The gut microbiota is highly responsive to changes in a wide range of environmental factors (for example, diet, drugs, stress). Thus, any manipulation or intervention aimed at studying the hypothalamus–gut microbiota axis may alter the microbiota composition, making it difficult to isolate specific cause-and-effect relationships. Another constraint is that, although our findings are probably applicable also to females, all studies conducted thus far have exclusively involved male mice. The effects of female hormones on gut microbiota have been reported in several species, including rodents and humans[36–39]. This poses challenges in controlling hormonal fluctuations and can represent a significant source of variability.

In summary, our findings uncover an unsuspected brain–gut connection that rapidly adjusts gut microbiota composition on short timescales, potentially participating in meal–meal adaptations and whole-body energy balance control. The identification of this new brain–gut axis represents an exciting point of departure in the field of neurogastroenterology and paves the way for new research to precisely delve into the mechanisms and their biological implications. Understanding this biological process may offer a potentially tractable target for a rapidly and transiently modulating gut microbiota composition. This approach would leverage the organism's own adaptive responses, holding potential benefits for metabolic disorders such as type 2 diabetes and obesity.

Methods

Mouse husbandry and diets

Animal studies followed the ethical standards approved by the Ethics Committee of the University of Barcelona (390/19) and the University of Santiago de Compostela (15012/2023/014) in compliance with local, national and European legislation. Mice were group-housed (4–5 animals per cage) under a controlled environment (humidity 30–80%; temperature 22–24 °C) under a 12-h light–dark cycle and with free access to water and standard diet (Teklad maintenance diet, 14% protein; 2014C, Envigo). In specific studies, HFD (60% kcal from fat, 4.7 kcal g^{-1}; cat. no. D12451, Research Diets) was provided ad libitum for 12 weeks (starting at 6 weeks of age). C57BL/6J, *POMC*$^{Cre/+}$[10] and *AgRP*$^{Cre/+}$ mice[9] were bred in-house. As controls, Cre^{-} littermates were used and maintained under identical conditions. For the chemogenetic experiments, all mice received CNO to control for potential ligand effects. Mice were randomly assigned to experimental treatments. Samples were consistently collected at the same time of day to ensure the replicability of microbiome analyses[40].

Food sensory paradigm

Eight-week-old C57BL/6J male mice were fasted overnight (16 h) and exposed to an inedible object (a wood dowel) or a standard chow pellet, both caged within a wire mesh that allowed the object or food to be seen and smelled but not consumed, as described previously[15]. Sixty minutes later, animals were euthanized for sample collection.

Stereotaxic surgery and cannulation

Eight-week-old C57BL/6J male mice (for the standard chow diet studies) or 18-week-old mice (for the HFD studies) were anaesthetized with 2.5% isoflurane in oxygen and placed in a stereotaxic frame. Head hair was shaved and the area cleaned with chlorhexidine. A stainless steel cannula was implanted in the right lateral ventricle (coordinates from Bregma: anteroposterior: −0.3 mm; mediolateral: +1.0 mm; dorsoventral: −2.5 mm below the surface of the skull) and fixed to the skull with *n*-butyl cyanoacrylate. To improve recovery, the area was treated with bupivacaine (local infiltration, 1.25 mg ml^{-1}); mice were placed on a heat pad (37 °C) until recovered from the anaesthesia.

Central hormonal treatments

The ICV leptin (L3772, Sigma-Aldrich) and ghrelin (4033076, Bachem) treatments were performed 3 days after cannula implantation. One hour after the start of the light period, mice were food-deprived for 2 h before treatment. At the time of the injection, the cannula was opened to administer leptin (3 µg per mouse), ghrelin (5 µg per mouse) or sterile saline for the controls, using a 25-µl syringe (Gas Tight Syringe, Hamilton Company). Animals were euthanized 2 or 4 h after the injection for sample collection.

Stereotaxic surgery for the chemogenetic studies

Eight-week-old *POMC*$^{Cre/+}$ and *AgRP*$^{Cre/+}$ male mice were anaesthetized intraperitoneally with ketamine/xylazine (100 mg kg^{-1} and 10 mg kg^{-1}) and placed in a stereotaxic frame (Kopf Instruments). For pain relief, mice received buprenorphine intraperitoneally (0.3 mg kg^{-1}) before surgery and every 12 h for 72 h after surgery. The skull was exposed and a small hole was drilled for AAV injection into the ARC. AAVs encoding excitatory (AAV8-hSYN-DIO-hM3D(Gq)-mCherry; 44361, Addgene; 1.10 × 1,013 gc ml^{-1}) or inhibitory (AAV8-hSYN-DIO-hM4D(Gi)-mCherry, 44362, Addgene; 1.10 × 1,013 gc ml^{-1}) DREADDs were injected bilaterally (300 nl per side) using a 33-G needle connected to a 5-µl syringe (NeuroSyringe, Hamilton Company) at 50 nl min^{-1} at the following

coordinates from Bregma: anteroposterior: −1.5 mm; mediolateral: ±0.3 mm; dorsoventral: −5.8 mm below the surface of the skull. After 8 min, the needle was retracted 1 mm and, after waiting 1 min, it was completely withdrawn. The incision was sutured with VetBond (3M) and mice were placed on a 37 °C heat pad until recovered from the anaesthesia. Experiments were conducted at least 3 weeks after the injections.

Chemogenetic activation or inhibition of POMC or AgRP neurons

On the experimental days, food was removed one hour after lights-on; 2 h later, mice were injected intraperitoneally with CNO (1 mg kg^{-1} for activation or 3 mg kg^{-1} for inhibition; C4936, Tocris Bioscience) dissolved in sterile saline. Mice were euthanized 2 or 4 h later. The correct injection sites were confirmed in every mouse postmortem by assessing the mCherry signal under a fluorescence microscope (Nikon Eclipse Ni-U).

Immunofluorescence studies

POMC$^{Cre/+}$ and *AgRP*$^{Cre/+}$ mice were anaesthetized with ketamine/xylazine and perfused intracardially with saline (PBS) followed by ice-cold 4% buffered paraformaldehyde. Brains were dissected, post-fixed overnight, cryoprotected with 30% sucrose, sectioned using a cryostat (RWD) at a 25-µm thickness; slices were stored at −20 °C.

For double POMC and FOS immunofluorescence in mCherry$^+$ specimens, hypothalamic slices containing the ARC were blocked with 2% donkey serum in KPBS + 0.1% Triton X-100 + 3% BSA and incubated overnight at 4 °C with rabbit anti-FOS antibody (1:300 dilution, 226008, Synaptic Systems) in blocking solution. After washing in KPBS + 0.1% Triton X-100, slices were incubated for 2 h with donkey anti-rabbit Alexa Fluor 647 antibody (1:300 dilution, A32795, Thermo Fisher Scientific) in KPBS + 0.1% Triton X-100 + 3% BSA. After washing in KPBS + 0.1% Triton X-100, slices were blocked with 2% donkey serum in KPBS + 0.4% Triton X-100 and incubated with rabbit anti-POMC precursor antibody (1:1,000 dilution; H-029-30, Phoenix Pharmaceuticals) for 16 h at 4 °C. Finally, slices were incubated with donkey anti-rabbit Alexa Fluor 488 antibody (1:200 dilution, Thermo Fisher Scientific) for 1.5 h at room temperature followed by nucleus counterstaining and mounting with ProLong Diamond Antifade mountant (P36971, Invitrogen). Imaging was performed using a Nikon Eclipse Ni-U fluorescence microscope. Representative images are maximum-intensity projections generated using ImageJ Fiji (National Institutes of Health) and equally adjusted for brightness and contrast. FOS$^+$POMC$^+$ neuron cells were manually counted in a blinded fashion using ImageJ Fiji. Three mice per genotype were analysed by averaging the percentage of FOS + POMC neurons across four images per mouse.

For FOS immunofluorescence in mCherry$^+$ specimens, hypothalamic slices containing the ARC were blocked with 2% donkey serum in KPBS + 0.1% Triton X-100 + 3% BSA and incubated with rabbit anti-FOS antibody (1:300 dilution, 226008, Synaptic Systems) in blocking solution overnight at 4 °C. After washing in KPBS + 0.1% Triton X-100, slices were incubated for 2 h with donkey anti-rabbit Alexa Fluor 488 antibody (1:300 dilution, A32790, Thermo Fisher Scientific) in KPBS + 0.1% Triton X-100 + 3% BSA, followed by nucleus counterstaining and mounting with ProLong Diamond Antifade mountant. Imaging was performed using a Nikon Eclipse Ni-U fluorescence microscope. Representative images are maximum-intensity projections generated using ImageJ Fiji and equally adjusted for brightness and contrast. FOS$^+$ neuron cells were manually counted in a blinded fashion using ImageJ Fiji. Three mice per genotype were analysed by averaging the percentage of FOS + POMC neurons across four images per mouse.

For the hormonal studies, C57BL/6J male mice were fasted 2 h before the ICV injection with vehicle, leptin or ghrelin. Ninety minutes after the injection, mice were anaesthetized with ketamine/xylazine and perfused intracardially with saline followed by ice-cold 10% neutral-buffered formalin. Brains were dissected and post-fixed overnight, cryoprotected with 30% sucrose, and cut using a cryostat (Epredia) at a 30-µm thickness; slices were stored at −20 °C. Hypothalamic slices containing the ARC were blocked with 2% goat serum in Tris-buffered saline (TBS) + 0.3% Triton X-100 + 0.25% BSA and incubated with chicken anti-FOS antibody (1:4,000 dilution, 226009, Synaptic Systems) in blocking solution overnight at 4 °C. After washing in TBS + 0.1% Triton X-100, slices were incubated for 2 h at room temperature with a goat anti-chicken Alexa Fluor 488 antibody (1:1,000 dilution, ab150169, Abcam) in TBS + 0.3% Triton X-100 + 0.25% BSA. Slices were washed with TBS + 0.1% Triton X-100 followed by nucleus counterstaining and mounting with Fluoro-Gel with Tris Buffer (17985-10, Electron Microscopy Sciences) + 4′,6-diamidino-2-phenylindole (1:1,000 dilution, cat. no. D9542, Sigma-Aldrich). Imaging was performed using a Leica TC-SP5-X-AOBS confocal microscope. Representative images were equally adjusted for brightness and contrast. Neuron cells positive for FOS were manually counted in a blinded fashion using ImageJ Fiji.

Body weight and blood glucose measurements

Body weight was measured using a precision scale. Blood samples were collected from the tail vein after overnight (16 h) fasting. The blood glucose concentration was measured using a glucose meter (Nova Pro Biomedical).

Leptin measurement

Leptin was measured in plasma using a Mouse/Rat Leptin Quantikine ELISA Kit (Bio-Techne). Blood samples were collected in Microvette 500 lithium heparin tubes and centrifuged at 2,000*g* for 15 min at 4 °C. Plasma was used for the analysis.

Gut motility measurements

Motility experiments were conducted according to a previously described protocol[41]. Briefly, cage food was removed 1 h after lights-on; 2 h later mice were injected intraperitoneally with CNO or ICV injected with ghrelin or leptin. Thirty minutes after CNO injection or 150 min after the hormonal interventions, each mouse received 200 µl of a sterile 5 mg ml^{-1} fluorescein isothiocyanate-dextran (70,000 MW, 46945, Sigma-Aldrich) solution in PBS, administered via oral gavage. Mice were euthanized 90 min later and gastrointestinal tracts were immediately collected and placed in ice-cold PBS for 30 s to inhibit motility. Tracts were dissected into 12 segments: stomach, small intestine (partitioned into eight equally sized segments) and colon (with caecum first dissected out; the remaining portion was divided into two equally sized segments). Each of the 12 segments was flushed with 2 ml of PBS. The intestinal flushes were subjected to serial dilutions. Fluorescence was measured using an Infinite M Nano+ 200 PRO (Tecan Ibérica Instrumentación). Absolute fluorescence levels were estimated using a dilution series of a fluorescein isothiocyanate-dextran solution of known concentration. Data analysis was performed as described in ref. 41.

Antibiotic treatment

Mice were treated with a combination of ampicillin and neomycin, two broad-spectrum antibiotics that are poorly (ampicillin) or not (neomycin) absorbed, thus minimizing systemic effects. One day after surgery, mice were divided into water or antibiotic treatment (ampicillin 1 g l^{-1}; neomycin 0.5 g l^{-1} in drinking water) groups. This procedure allowed us to investigate the contribution of the gut microbiota to the host phenotype[42–44]. After 48 h of treatment, saline or leptin (3 µg) was delivered ICV and mice were euthanized 2 h later. The duodenum was collected and snap-frozen in liquid nitrogen. Frozen samples were processed for RNA isolation and RNA-seq as described below.

Catecholamine measurement

Catecholamines were measured in duodenal sections using an Epinephrine/Norepinephrine ELISA Kit (2-CAT High Sensitive ELISA BA E-5400R, Labor Diagnostika Nord). For extraction, tissues were digested in 0.01 N

HCl-0.3 mg ml^{-1} ascorbic acid buffer using a homogenizer. Samples were centrifuged at 3,400*g* for 20 min at 4 °C and the supernatants were used for subsequent analysis.

16S rRNA gene sequencing of intestinal luminal content

Samples of mucus and luminal content were collected from the duodenum, jejunum, ileum and caecum of each mouse at selected time points for subsequent analysis of microbiota composition. Metagenomic DNA was extracted using a QIAamp Fast DNA Stool Mini Kit (cat. no. 51604, QIAGEN), according to the manufacturer's instructions with minor modifications[45].

Library preparation and sequencing of the V4 variable region of the 16S rRNA gene was performed by the Mr. DNA Lab, using the illCUs515F (GTGYCAGCMGCCGCGGTAA) and new806RB (GGACTACNVGGGTWTCTAAT) primer pair and 2 × 250 bp paired-end Illumina MiSeq sequencing technology (30 cycles). FASTQ data of demultiplexed samples were downloaded from the Illumina BaseSpace Sequence Hub using the BaseMount tool.

Paired-end reads were merged using USEARCH[46,47] with a maximum number of ten mismatches in the alignment. VSEARCH[48] was used to strip primer sequences, globally trim the reads to 252 bp and filter the reads using an expected error threshold of 1. Reads containing wildcard bases were removed. Dereplication was performed, after which the unique sequences were denoised with UNOISE3 (ref. 49). Trimmed and quality-filtered reads were aligned with VSEARCH using a pairwise 97% sequence identity threshold onto the predicted zero-radius operational taxonomic unit (ZOTU) sequences to generate an OTU table. The table was converted to the BIOM format[50]. SINTAX was used to taxonomically classify the ZOTU sequences[51] with the Ribosomal Database Project Training Set v.18 and a bootstrap cut-off value of 0.8.

Analysis of gut microbiota composition and abundance

We began by merging the working tables into a phyloseq R package object per experiment (v.4.0.3) (https://www.R-project.org/), including sample, taxonomic classification and count data. To minimize host DNA contamination, we preprocessed the data to work with bacteria only. We also removed taxa with Cyanobacteria phylum annotations to avoid food and water contamination biases. One technical outlier (total counts below 30,000) was removed (Supplementary Fig. 1). No biological outliers were based on (1) extremely different α-diversity score and (2) clear dissimilarities in the principal coordinate analysis distribution compared with the rest of the group components (based on Bray–Curtis dissimilarity).

The statistical analysis included clustering, α-diversity, β-diversity and effect size analysis; α-diversity was conducted using ZOTUs, completed by first rarefying the samples library sizes in each experiment to the minimum sample depth of that experiment without replacement. This was implemented using the phyloseq R package. The Shannon index was used to represent α-diversity along with the application of a linear model, followed by an ANOVA and FDR post-hoc adjustment (using the stats and car R packages). Data clustering was conducted using principal coordinate analysis of all data (using the phyloseq R package), including gut section, activation or treatment by tissue section or taxa. Differential abundance analysis for each gut segment, time point and treatment was performed to obtain the differential abundant taxa by implementing the ANCOM-BC method (using the ancombc function from the ANCOM-BC R package)[11]. ANCOM-BC uses log-ratio transformation and corrects the bias induced by the differences among samples. Absolute abundance data were modelled using a linear regression framework. The method also accounted for zero inflation. To control the FDR across tests, the Benjamini–Hochberg correction was applied, with taxa considered significantly different when P_{adj} (q) was less than 0.05. Data visualization was performed using the RColorBrewer, ggplot2, pheatmap and circlize packages in R.

Prediction of microbial metabolic functions

PICRUSt2 (ref. 52) was used to predict the metabolic signatures of the microbial communities within the QIIME2 environment[52]. Rarefied pathway abundances were further analysed in STAMP[53] using a Welch test between groups. The MetaCyc Metabolic Pathway Database was used to decipher the ontology of pathways.

Metabolomics

A Dionex Ultimate 3000 RS LC system coupled to an Orbitrap mass spectrometer (Q Exactive, ThermoHESI-II Fisher Scientific) equipped with a heated electrospray ionization (HESI-II) probe was used. Solvents were of LC–MS grade quality (Merck). The luminal content from the duodenum was collected 4 h after leptin treatment and stored at −80 °C until analysis. Metabolomic profiling was performed as reported previously with minor variations[54]. Briefly, 50 µl of water and 700 µl of acetone, acetonitrile and methanol (1:1:1, v/v/v), containing 2.5 µM Metabolomics Amino Acid Mix Standard (Cambridge Isotope Laboratories), were added to each sample (34 ± 8.6 mg). After incubation and centrifugation, 600 µl of the supernatant were dried under vacuum. The leftover supernatants of all samples were pooled and used for the quality control (QC) samples. Dried supernatants were reconstituted in 70 µl of methanol and acetonitrile (1:1, v/v) for LC–MS/MS analysis.

Metabolites were separated on a SeQuant ZIC-HILIC column (150 × 2.1 mm, 5 µm; Merck) using water with 5 mM ammonium acetate as eluent A and acetonitrile/eluent A (95:5, v/v) as eluent B, both containing 0.1% formic acid. The gradient elution was set as follows: isocratic step of 100% B for 3 min, 100% B to 60% B in 15 min, held for 5 min, returned to initial conditions in 5 min and held for 5 min. The flow rate was 0.5 ml min^{-1}. Data acquisition was carried out with data-dependent MS/MS scans (top ten).

Compound Discoverer 3.3 (Thermo Fisher Scientific) was used for data processing. Metabolites were identified based on exact mass, retention time, fragmentation spectra and isotopic pattern. We used an in-house fragmentation library[54], a microbiome-specific library[55] and the online library mzCloud. QC-based normalization was performed. The area under the peak was additionally normalized to the appropriate internal standard and sample weight. QC at four concentrations ensured signal stability and linearity. Partial least squares discriminant analysis was conducted using the mixOmics package (v.6.28.0) in R. Group differences were assessed using the Mann–Whitney *U*-test and FDR correction. Metabolites were considered significant when P_{adj} (q) was less than 0.05 and the absolute fold change greater than 1.25. Visualizations were generated using the ggplot2 package in R.

Neuroactive potential

Gut–brain modules (GBMs) were inferred as described in ref. 24. Briefly, GBMs were inferred from the orthologue abundance table obtained with PICRUSt2, using the web application GOmixer (http://www.raeslab.org/gomixer/). The detection threshold was set at 66% coverage and a minimum median difference of 5.0. Data were scaled according to sample abundance and the mean of observed reactions was used as an abundance estimator. GBMs were considered significant when $P < 0.05$ and were represented using the ggplot2 package in R.

RNA-seq and analysis

Duodenal mRNA was isolated using the TRIzol reagent (cat. no. 15596026, Invitrogen) according to standard protocols. Quantification and integrity analysis of RNA were performed using an Agilent 2100 Bioanalyzer (Agilent RNA 6000 Nano Kit, Agilent Technologies). Strand-specific RNA libraries were generated using 150 ng of total RNA with the Illumina Stranded RNA Prep Ligation Kit with Ribo-Zero Plus according to the manufacturer's instructions. Libraries were sequenced on an Illumina NextSeq 2000 in paired-end mode (read length of 2 × 50 bp). Forty million paired-end reads were generated

for each sample and condition. Sequencing was conducted at the Genomics Facility of the Institut d'Investigacions Biomèdiques August Pi i Sunyer.

Raw reads passed the QC established in the FastQC software (http://www.bioinformatics.babraham.ac.uk/projects/fastqc) and mapped to the reference genome mm10 using HISAT[56]. Gene counts were acquired using featureCounts[57]. The expression read matrix cut-off was set at an average of ten and read counts were normalized to counts per million using the R package EdgeR (v.3.42.0). Differentially expressed genes (DEGs) were calculated using the limma (v.3.60.4) R package from Bioconductor, applying batch correction. Significant DEGs were those with $P < 0.05$ and an absolute fold change value greater than 1.5. A principal component analysis plot was generated using the ggfortify (v.0.4.16) and ggplot2 (v.3.4.4) R packages. Pathway enrichment analysis of the DEGs was performed using AmiGO 2 (https://amigo.geneontology.org/amigo); significant annotations ($P < 0.05$) were selected. The top 50 significant pathways were manually curated into biological categories represented in the Sankey plot generated using the ggaluvial (v.0.12.5) R package.

Statistical analysis

We used statistical methods (https://www.datarus.eu/en/applications/granmo/) along with previous experience to predetermine sample sizes. Data collection and analysis were not performed blind to the conditions of the experiments, except for image acquisition and analysis. Data exclusion was based on the ROUT method (1% threshold). Data are presented as the mean ± s.e.m. or as individual biological replicates. Statistical analyses were performed using Prism 8.0 (GraphPad Software) and R v.4.4.0. Data distribution was assumed to be normal. Statistical significance was determined with an unpaired one-tailed or two-tailed Student's *t*-test, one-way or two-way ANOVA followed by an appropriate post-hoc test, as indicated in the figure legends. The number of samples (n) are indicated in the figure legends. $P \leq 0.05$ was considered statistically significant.

Reporting summary

Further information on research design is available in the Nature Portfolio Reporting Summary linked to this article.

Data availability

The RNA-seq datasets generated and analysed during the study are available at the Gene Expression Omnibus repository under accession no. GSE266230. The clean reads were mapped to the reference genome assembly GRCm38 from GCA_000001635.2. The metagenomic data have been deposited in the Sequence Read Archive under accession no. PRJNA1107501. The metabolomics data have been deposited in the Metabolomics Workbench under project no. PR002229. Source data are provided with this paper.

References

1. Van Hul, M. et al. What defines a healthy gut microbiome? *Gut* **73**, 1893–1908 (2024).
2. Dalile, B., Van Oudenhove, L., Vervliet, B. & Verbeke, K. The role of short-chain fatty acids in microbiota–gut–brain communication. *Nat. Rev. Gastroenterol. Hepatol.* **16**, 461–478 (2019).
3. Agus, A., Clément, K. & Sokol, H. Gut microbiota-derived metabolites as central regulators in metabolic disorders. *Gut* **70**, 1174–1182 (2021).
4. Brüning, J. C. & Fenselau, H. Integrative neurocircuits that control metabolism and food intake. *Science* **381**, eabl7398 (2023).
5. Mirabella, P. N. & Fenselau, H. Advanced neurobiological tools to interrogate metabolism. *Nat. Rev. Endocrinol.* **19**, 639–654 (2023).
6. Cani, P. D. Microbiota and metabolites in metabolic diseases. *Nat. Rev. Endocrinol.* **15**, 69–70 (2019).
7. Breton, J. et al. Gut commensal *E. coli* proteins activate host satiety pathways following nutrient-induced bacterial growth. *Cell Metab.* **23**, 324–334 (2016).
8. Furness, J. B., Callaghan, B. P., Rivera, L. R. & Cho, H.-J. The enteric nervous system and gastrointestinal innervation: integrated local and central control. *Adv. Exp. Med. Biol.* **817**, 39–71 (2014).
9. Tong, Q., Ye, C.-P., Jones, J. E., Elmquist, J. K. & Lowell, B. B. Synaptic release of GABA by AgRP neurons is required for normal regulation of energy balance. *Nat. Neurosci.* **11**, 998–1000 (2008).
10. Xu, A. W. et al. PI3K integrates the action of insulin and leptin on hypothalamic neurons. *J. Clin. Invest.* **115**, 951–958 (2005).
11. Lin, H. & Peddada, S. D. Analysis of compositions of microbiomes with bias correction. *Nat. Commun.* **11**, 3514 (2020).
12. Chen, Y., Lin, Y.-C., Kuo, T.-W. & Knight, Z. A. Sensory detection of food rapidly modulates arcuate feeding circuits. *Cell* **160**, 829–841 (2015).
13. Betley, J. N. et al. Neurons for hunger and thirst transmit a negative-valence teaching signal. *Nature* **521**, 180–185 (2015).
14. Mandelblat-Cerf, Y. et al. Arcuate hypothalamic AgRP and putative POMC neurons show opposite changes in spiking across multiple timescales. *eLife* **4**, e07122 (2015).
15. Brandt, C. et al. Food perception primes hepatic ER homeostasis via melanocortin-dependent control of mTOR activation. *Cell* **175**, 1321–1335 (2018).
16. Timper, K. & Brüning, J. C. Hypothalamic circuits regulating appetite and energy homeostasis: pathways to obesity. *Dis. Model. Mech.* **10**, 679–689 (2017).
17. Yarandi, S. S., Hebbar, G., Sauer, C. G., Cole, C. R. & Ziegler, T. R. Diverse roles of leptin in the gastrointestinal tract: modulation of motility, absorption, growth, and inflammation. *Nutrition* **27**, 269–275 (2011).
18. Douglas, G. M. et al. PICRUSt2 for prediction of metagenome functions. *Nat. Biotechnol.* **38**, 685–688 (2020).
19. Langille, M. G. I. et al. Predictive functional profiling of microbial communities using 16S rRNA marker gene sequences. *Nat. Biotechnol.* **31**, 814–821 (2013).
20. Frost, G. et al. The short-chain fatty acid acetate reduces appetite via a central homeostatic mechanism. *Nat. Commun.* **5**, 3611 (2014).
21. Kasaoka, S. et al. Histidine supplementation suppresses food intake and fat accumulation in rats. *Nutrition* **20**, 991–996 (2004).
22. Alamshah, A. et al. L-arginine promotes gut hormone release and reduces food intake in rodents. *Diabetes Obes. Metab.* **18**, 508–518 (2016).
23. Blouet, C., Jo, Y.-H., Li, X. & Schwartz, G. J. Mediobasal hypothalamic leucine sensing regulates food intake through activation of a hypothalamus–brainstem circuit. *J. Neurosci.* **29**, 8302–8311 (2009).
24. Valles-Colomer, M. et al. The neuroactive potential of the human gut microbiota in quality of life and depression. *Nat. Microbiol.* **4**, 623–632 (2019).
25. Martinez-Sanchez, N. et al. The sympathetic nervous system in the 21st century: neuroimmune interactions in metabolic homeostasis and obesity. *Neuron* **110**, 3597–3626 (2022).
26. Bell, B. B. et al. Differential contribution of POMC and AgRP neurons to the regulation of regional autonomic nerve activity by leptin. *Mol. Metab.* **8**, 1–12 (2018).
27. Nogueiras, R. et al. The central melanocortin system directly controls peripheral lipid metabolism. *J. Clin. Invest.* **117**, 3475–3488 (2007).
28. Thaiss, C. A. et al. Transkingdom control of microbiota diurnal oscillations promotes metabolic homeostasis. *Cell* **159**, 514–529 (2014).
29. Liang, X., Bushman, F. D. & FitzGerald, G. A. Rhythmicity of the intestinal microbiota is regulated by gender and the host circadian clock. *Proc. Natl Acad. Sci. USA* **112**, 10479–10484 (2015).

30. Zarrinpar, A., Chaix, A., Yooseph, S. & Panda, S. Diet and feeding pattern affect the diurnal dynamics of the gut microbiome. *Cell Metab.* **20**, 1006–1017 (2014).
31. David, L. A. et al. Diet rapidly and reproducibly alters the human gut microbiome. *Nature* **505**, 559–563 (2014).
32. Houlden, A. et al. Brain injury induces specific changes in the caecal microbiota of mice via altered autonomic activity and mucoprotein production. *Brain Behav. Immun.* **57**, 10–20 (2016).
33. Galley, J. D. et al. Exposure to a social stressor disrupts the community structure of the colonic mucosa-associated microbiota. *BMC Microbiol.* **14**, 189 (2014).
34. Chang, H. et al. Stress-sensitive neural circuits change the gut microbiome via duodenal glands. *Cell* **187**, 5393–5412 (2024).
35. Woods, S. C. The eating paradox: how we tolerate food. *Psychol. Rev.* **98**, 488–505 (1991).
36. Koren, O. et al. Host remodeling of the gut microbiome and metabolic changes during pregnancy. *Cell* **150**, 470–480 (2012).
37. Org, E. et al. Sex differences and hormonal effects on gut microbiota composition in mice. *Gut Microbes* **7**, 313–322 (2016).
38. Park, S., Kim, D. S., Kang, E. S., Kim, D. B. & Kang, S. Low-dose brain estrogen prevents menopausal syndrome while maintaining the diversity of the gut microbiomes in estrogen-deficient rats. *Am. J. Physiol. Endocrinol. Metab.* **315**, E99–E109 (2018).
39. Nuriel-Ohayon, M. et al. Progesterone increases *Bifidobacterium* relative abundance during late pregnancy. *Cell Rep.* **27**, 730–736 (2019).
40. Allaband, C. et al. Time of sample collection is critical for the replicability of microbiome analyses. *Nat. Metab.* **6**, 1282–1293 (2024).
41. Koester, S. T., Li, N., Lachance, D. M. & Dey, N. Marker-based assays for studying gut transit in gnotobiotic and conventional mouse models. *STAR Protoc.* **2**, 100938 (2021).
42. Cani, P. D. et al. Changes in gut microbiota control metabolic endotoxemia-induced inflammation in high-fat diet-induced obesity and diabetes in mice. *Diabetes* **57**, 1470–1481 (2008).
43. Muccioli, G. G. et al. The endocannabinoid system links gut microbiota to adipogenesis. *Mol. Syst. Biol.* **6**, 392 (2010).
44. Vijay-Kumar, M. et al. Metabolic syndrome and altered gut microbiota in mice lacking Toll-like receptor 5. *Science* **328**, 228–231 (2010).
45. Everard, A. et al. Microbiome of prebiotic-treated mice reveals novel targets involved in host response during obesity. *ISME J.* **8**, 2116–2130 (2014).
46. Edgar, R. C. Search and clustering orders of magnitude faster than BLAST. *Bioinformatics* **26**, 2460–2461 (2010).
47. Edgar, R. C. & Flyvbjerg, H. Error filtering, pair assembly and error correction for next-generation sequencing reads. *Bioinformatics* **31**, 3476–3482 (2015).
48. Rognes, T., Flouri, T., Nichols, B., Quince, C. & Mahé, F. VSEARCH: a versatile open source tool for metagenomics. *PeerJ* **4**, e2584 (2016).
49. Edgar R. C. UNOISE2: improved error-correction for Illumina 16S and ITS amplicon sequencing. Preprint at *bioRxiv* https://doi.org/10.1101/081257 (2016).
50. McDonald, D. et al. The Biological Observation Matrix (BIOM) format or: how I learned to stop worrying and love the ome-ome. *Gigascience* **1**, 7 (2012).
51. Edgar R. C. SINTAX: a simple non-Bayesian taxonomy classifier for 16S and ITS sequences. Preprint at *bioRxiv* https://doi.org/10.1101/074161 (2016).
52. Bolyen, E. et al. Reproducible, interactive, scalable and extensible microbiome data science using QIIME 2. *Nat. Biotechnol.* **37**, 852–857 (2019).
53. Parks, D. H., Tyson, G. W., Hugenholtz, P. & Beiko, R. G. STAMP: statistical analysis of taxonomic and functional profiles. *Bioinformatics* **30**, 3123–3124 (2014).
54. Folberth, J., Begemann, K., Jöhren, O., Schwaninger, M. & Othman, A. MS2 and LC libraries for untargeted metabolomics: enhancing method development and identification confidence. *J. Chromatogr. B* **1145**, 122105 (2020).
55. Han, S. et al. A metabolomics pipeline for the mechanistic interrogation of the gut microbiome. *Nature* **595**, 415–420 (2021).
56. Kim, D., Langmead, B. & Salzberg, S. L. HISAT: a fast spliced aligner with low memory requirements. *Nat. Methods* **12**, 357–360 (2015).
57. Liao, Y., Smyth, G. K. & Shi, W. featureCounts: an efficient general purpose program for assigning sequence reads to genomic features. *Bioinformatics* **30**, 923–930 (2014).

Acknowledgements

The project leading to these results received funding from 'la Caixa' Foundation (ID100010434) under project no. LCF/PR/HR19/52160016 (to M.C., R.N. and P.D.C.), with the support of Project 2021-SGR-01320 from the Generalitat de Catalunya, Departament de Recerca i Universitats and the CERCA Programme/Generalitat de Catalunya (to M.C.), and a European Research Council ERC-Synergy-Grant-2019-WATCH no. 810331 (to R.N. and M.S.). M.T. is a recipient of a Beatriu de Pinós postdoctoral fellowship (2018 BP00032), funded by the Secretary of Universities and Research (Government of Catalonia), and by the Horizon 2020 programme of the European Union under a Marie Skłodowska-Curie grant no. 801370, as well as a contract funded by the Instituto de Salud Carlos III with European funds from the Recovery, Transformation, and Resilience Plan, under file code IHMC22/00039 and Funded by the European Union-Next Generation EU. I.M-I. was supported by the Miguel Servet Type II program (CPII21/00013) of the ISCIII-Madrid (Spain) and co-funded by the European Union. A.O. is the recipient of a Miguel Servet contract (no. CP19/00083) funded by the Instituto de Salud Carlos III and co-funded by the European Social Fund 'Investing in your future'. R.H-T. is a recipient of a Ramon y Cajal contract (no. RYC2022-037070-I) from the Ministerio de Ciencia e Innovación of Spain. P.D.C. is an honorary research director at the Fonds de la Recherche Scientifique/Fonds National de la Recherche Scientifique and recipient of a Fonds de la Recherche Fondamentale Stratégique-Walloon Excellence in Life Sciences and BIO (WELBIO) technology WELBIO grant no. WELBIO-CR-2022A-02 and EOS program no. 40007505. We are indebted to the Functional Genomics Core Facility of the Institut d' Investigacions Biomèdiques August Pi i Sunyer for their technical help. This work was carried out in part at the Esther Koplowitz Centre, Barcelona.

Author contributions

M.T., S.M-M. and M.V.H. designed and conducted the experiments, analysed the results and contributed to paper preparation. B.L., E.E., R.P., J.A., J.I., I.M-I. and S.R.L. conducted the biostatistics and bioinformatics analyses. A.P., A.G.G-V, J.I., M.P., I.C., M.M-G., S.R., R.H-T., A.O., J.F-D., I.T., E.M. and M.S. contributed to conducting the experimental procedures and analysis. P.D.C., R.N. and M.C. conceived the study, designed, coordinated and supervised experiments, wrote the paper and secured the funding. All authors discussed the results, commented on the paper before submission and agreed with the final submitted paper.

Competing interests

P.D.C. is the inventor in patent applications dealing with the use of specific bacteria and components in the treatment of different diseases. P.D.C. was co-founder of the Akkermansia Company and Enterosys. Rubén Nogueiras serves in the Advisory Board of Albor Biotech. The other authors declare no competing interests.

Additional information

Extended data is available for this paper at https://doi.org/10.1038/s42255-025-01280-3.

Supplementary information The online version contains supplementary material available at https://doi.org/10.1038/s42255-025-01280-3.

Correspondence and requests for materials should be addressed to Patrice D. Cani, Rubén Nogueiras or Marc Claret.

Peer review information *Nature Metabolism* thanks John Cryan and the other, anonymous, reviewer(s) for their contribution to the peer review of this work. Primary Handling Editor: Alfredo Giménez-Cassina, in collaboration with the *Nature Metabolism* team.

Míriam Toledo[1], Sara Martínez-Martínez[2], Matthias Van Hul[3,4], Berta Laudo[1], Elena Eyre[1], Rudy Pelicaen[3], Anthony Puel[3,4], Jordi Altirriba[5], Alicia G. Gómez-Valadés[1], Julica Inderhees[6,7], Isabel Moreno-Indias[8,9], Macarena Pozo[1], Iñigo Chivite[1], Maria Milà-Guasch[1], Roberta Haddad-Tóvolli[1], Arnaud Obri[1], Júlia Fos-Domènech[1], Iasim Tahiri[1], Sergio R. Llana[1], Sara Ramírez[1], Erika Monelli[1], Markus Schwaninger[7,10], Patrice D. Cani[3,4,11,15] ✉, Rubén Nogueiras[2,9,12,15] ✉ & Marc Claret[1,13,14,15] ✉

[1]Neuronal Control of Metabolism Laboratory, Institut d'Investigacions Biomèdiques August Pi i Sunyer (IDIBAPS), Barcelona, Spain. [2]Department of Physiology (CIMUS), School of Medicine-Instituto de Investigaciones Sanitarias (IDIS), Universidad de Santiago de Compostela, Santiago de Compostela, Spain. [3]Metabolism and Nutrition Research Group (MNUT), Louvain Drug Research Institute (LDRI), UCLouvain, Université Catholique de Louvain, Brussels, Belgium. [4]Walloon Excellence in Life Sciences and BIOtechnology (WELBIO), WELBIO department, WEL Research Institute, Wavre, Belgium. [5]Laboratory of Metabolism, Department of Internal Medicine Specialties, Faculty of Medicine, University of Geneva, Geneva, Switzerland. [6]Bioanalytic Core Facility, Center for Brain, Behavior and Metabolism, University of Lübeck, Lübeck, Germany. [7]German Research Centre for Cardiovascular Research (DZHK), Lübeck, Germany. [8]Department of Endocrinology and Nutrition, Instituto de Investigación Biomédica de Málaga y Plataforma en Nanomedicina-IBIMA Plataforma Bionand, Málaga, Spain. [9]CIBER Fisiopatologia de la Obesidad y Nutrición (CIBERobn), Santiago de Compostela, Spain. [10]Institute of Experimental and Clinical Pharmacology and Toxicology, Center of Brain, Behavior and Metabolism (CBBM), University of Lübeck, Lübeck, Germany. [11]Institute of Experimental and Clinical Research (IREC), UCLouvain, Université Catholique de Louvain, Brussels, Belgium. [12]Galicia Agency of Innovation (GAIN), Xunta de Galicia, Santiago de Compostela, Spain. [13]CIBER de Diabetes y Enfermedades Metabólicas Asociadas (CIBERDEM), Barcelona, Spain. [14]School of Medicine, Universitat de Barcelona, Barcelona, Spain. [15]These authors contributed equally: Patrice D. Cani, Rubén Nogueiras, Marc Claret. ✉e-mail: patrice.cani@uclouvain.be; ruben.nogueiras@usc.es; mclaret@recerca.clinic.cat

https://doi.org/10.1038/s42255-025-01280-3

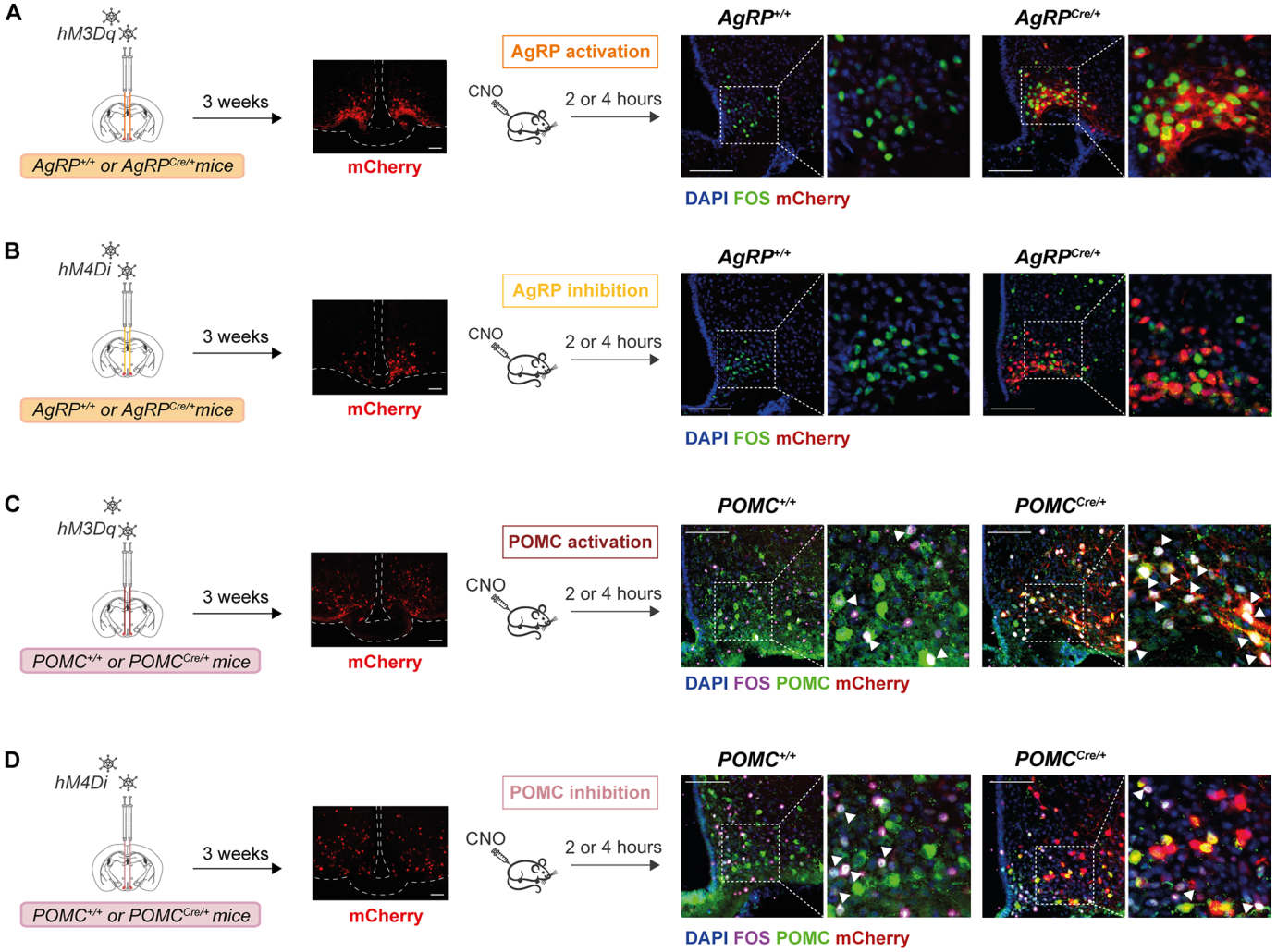

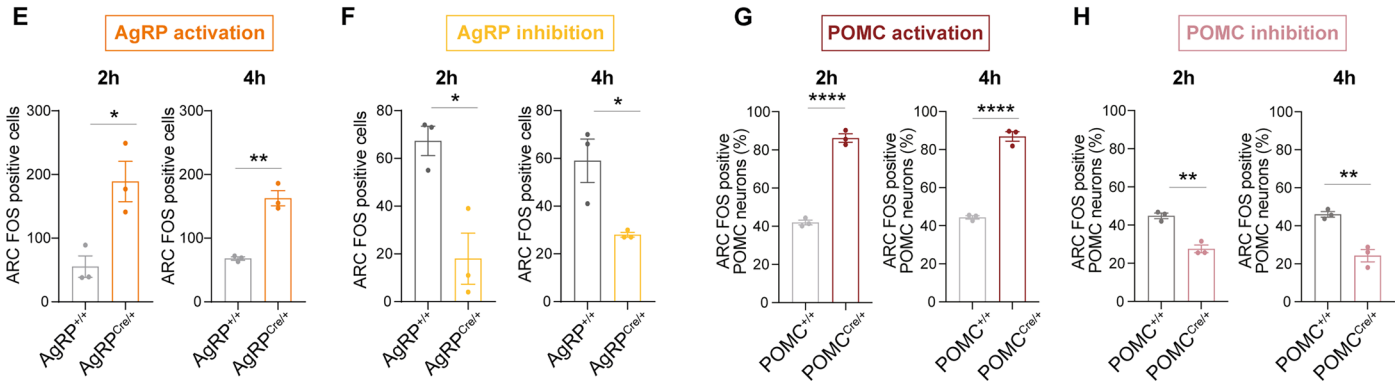

Extended Data Fig. 1 | Assessment of chemogenetic modulation of AgRP and POMC neurons. a–d. Schematic of the approach to express the excitatory (hM3Dq) or inhibitory DREADDs (hM4Di) in AgRP and POMC neurons ($n = 3$ mice per group). The representative images show mCherry reporter expression in ARC coronal sections. **a, b.** Assessment of chemogenetic activation (A) or inhibition (B) of AgRP neurons in AgRP$^{+/+}$ and AgRP$^{Cre/+}$ mice expressing hM3Dq or hM4Di two hours after CNO injection. Representative images of FOS (green), mCherry (red), and DAPI nuclei counterstaining (blue) are shown. Scale bar: 50 µm. **c, d.** Assessment of chemogenetic activation (C) or inhibition (D) of POMC neurons in POMC$^{+/+}$ and POMC$^{Cre/+}$ mice expressing hM3Dq or hM4Di two hours after CNO injection. Representative images of FOS (magenta) and POMC (green) immunostaining, mCherry (red) and DAPI nuclei counterstaining (blue) are shown. Scale bar: 50 µm. **e, f.** Quantification of FOS-positive cells in AgRP$^{+/+}$ and AgRP$^{Cre/+}$ mice expressing hM3Dq ($n = 3$ mice per group) (E; *p = 0.0205 hM3Dq, 2 h; **p = 0.0015 hM3Dq, 4 h) or hM4Di (F; *p = 0.0162 hM4Di, 2 h; *p = 0.0274 hM4Di, 4 h) two or four hours after CNO injection. **g, h.** Quantification of FOS-positive POMC neurons in POMC$^{+/+}$ and POMC$^{Cre/+}$ mice expressing hM3Dq ($n = 3$ mice per group) (G; ****p < 0.0001 hM3Dq, 2 h; ****p < 0.0001 hM3Dq, 4 h) or hM4Di (H; **p = 0.0022 hM4Di, 2 h; **p = 0.037 hM4Di, 4 h) two or four hours after CNO injection. Statistical significance was determined with a two-tailed *t* test. hM3Dq: AAV8-hSYN-DIO-hM3D(Gq)mCherry; hM4Di: AAV8-hSYN-DIO-hM4D(Gi)mCherry; CNO: Clozapine-N-Oxide. Data in panels E-H are represented as mean ± SEM.

https://doi.org/10.1038/s42255-025-01280-3

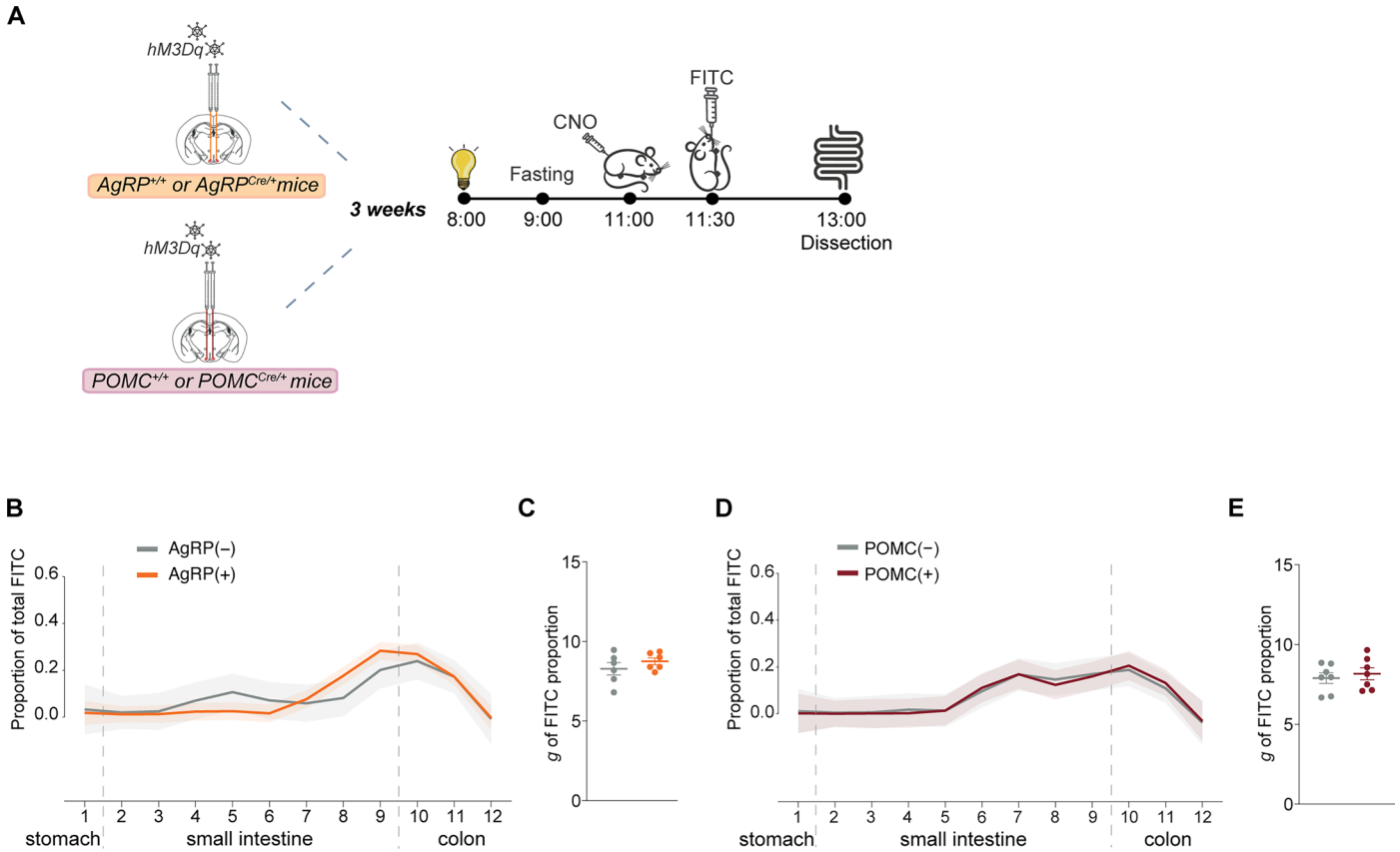

Extended Data Fig. 2 | Modulation of AgRP or POMC neuron activity does not induce alterations in gut motility. a. Diagram illustrating the experimental outline for the analysis of gut motility. **b**–**e.** Loess curve of intestinal FITC distributions after chemogenetic activation of AgRP (B-C; $n = 6$ mice per group) and POMC (D-E; $n = 7$ mice in POMC(-) group and $n = 8$ mice in POMC(+) group) neurons. X-axis represents different gut segments from stomach to colon. Dot plots represent the geometric mean (g) of FITC proportion. Data are represented as mean ± SEM. Statistical significance was determined using the Wilcoxon test, followed by Benjamini-Hochberg correction. CNO: Clozapine-N-Oxide. FITC: Fluorescein Isothiocyanate.

https://doi.org/10.1038/s42255-025-01280-3

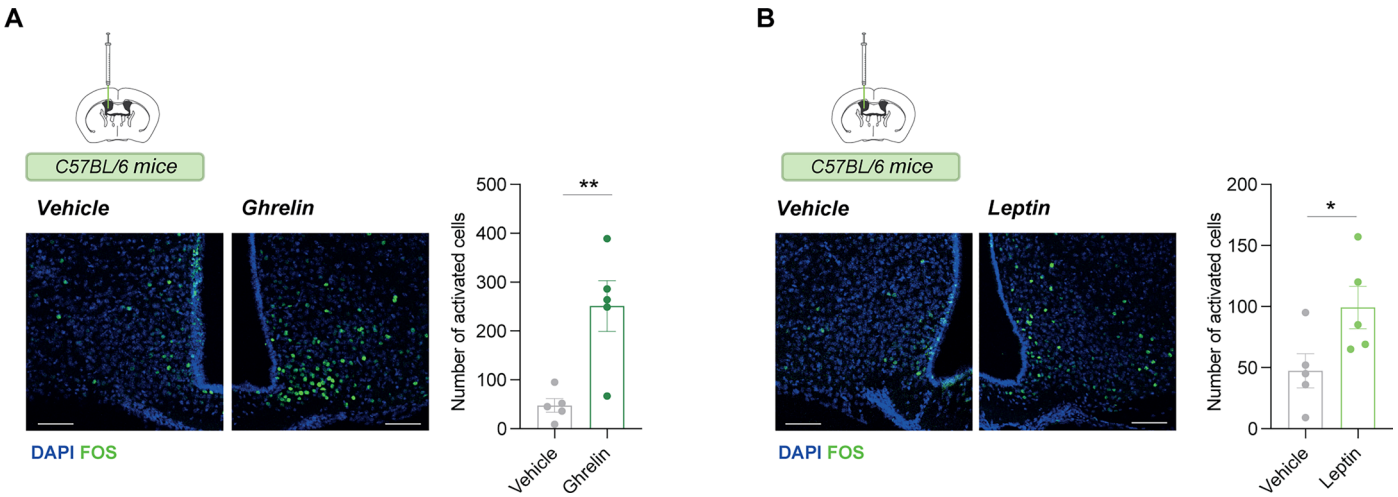

Extended Data Fig. 3 | Validation of neuronal activity after central ghrelin or leptin administration. a, b. Representative immunofluorescence images showing FOS staining (green) in the arcuate nucleus of the hypothalamus after intracerebroventricular delivery of ghrelin (A) or leptin (B) (n = 5 mice per group). Nuclei were stained with DAPI (blue). Scale bar: 100 µm. Quantification is also shown. Data is represented as mean ± SEM. Statistical significance was determined with a one-tailed t test. *p = 0.0244, **p = 0.0027.

https://doi.org/10.1038/s42255-025-01280-3

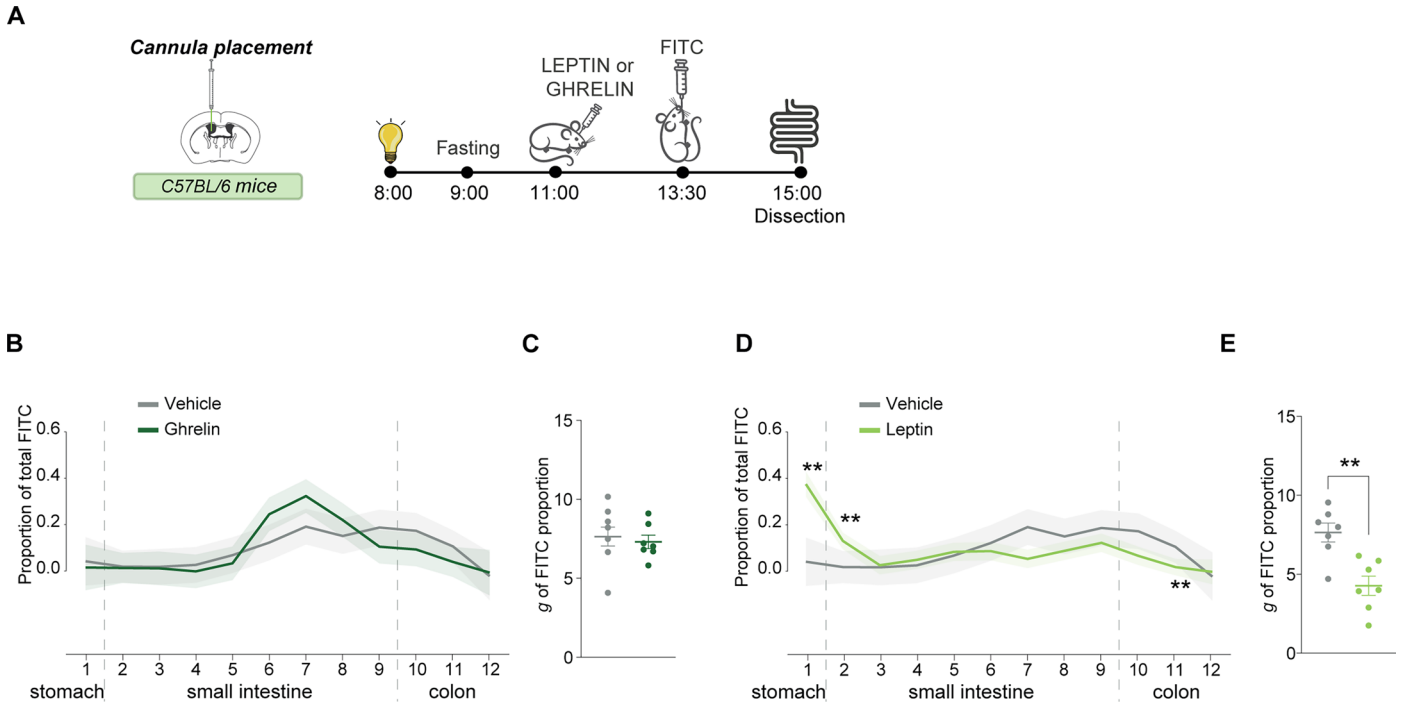

Extended Data Fig. 4 | Central leptin administration modulates gut motility. **a**. Diagram illustrating the experimental outline for the analysis of gut motility. **b**–**e**. Loess curve of intestinal FITC distributions after intracerebroventricular ghrelin (**b, c**) and leptin (**d, e**) administration ($n = 7$ mice per group). X-axis represents different gut segments from stomach to colon. Dot plots represent the geometric mean (g) of FITC proportion. Data are represented as mean ± SEM. Statistical significance was determined using the Wilcoxon test, followed by Benjamini-Hochberg correction. D, section 1, **p = 0.002; section 2, **p = 0.002; section 11, **p = 0.009. E, **p = 0.0041. FITC: Fluorescein Isothiocyanate.

https://doi.org/10.1038/s42255-025-01280-3

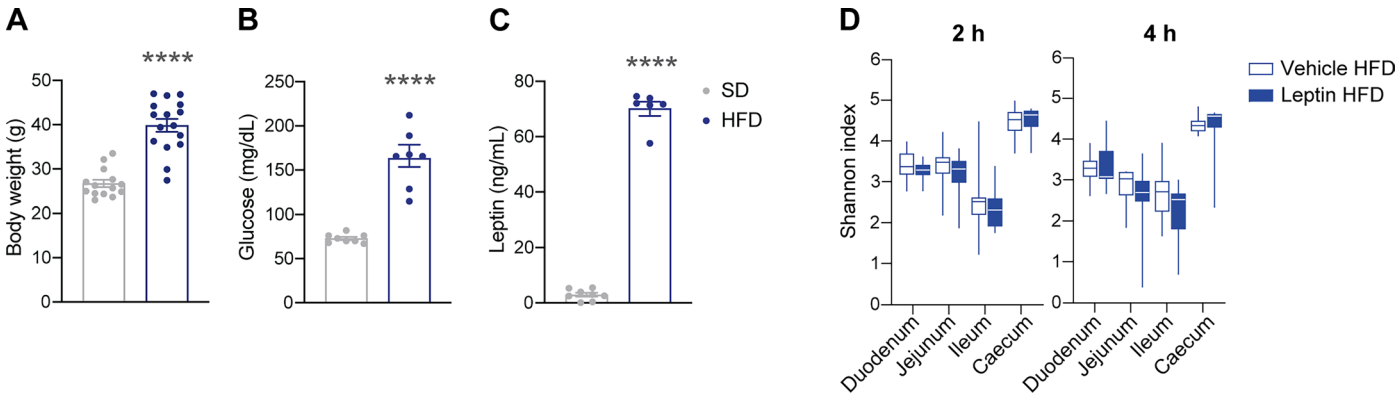

Extended Data Fig. 5 | High fat diet feeding causes overweight, hyperglycaemia and plasma hyperleptinemia. a–c. Body weight (A), blood glucose (B), and plasma leptin levels (C) of mice fed with a standard diet (SD) or a high-fat diet (HFD) for 12 weeks. Data is represented as mean ± SEM (A, SD $n = 14$ mice and HFD $n = 16$ mice; B, SD $n = 8$ mice and HFD $n = 7$ mice; C, SD $n = 8$ mice and HFD $n = 6$ mice). Statistical significance was determined with a two-tailed t test. ****$p < 0.0000$. **d.** Microbial α-diversity (Shannon index) of the gut microbiota in vehicle- and centrally leptin-treated mice following 12 weeks of HFD, assessed at two- and four-hours post-treatment ($n = 10$ mice per group). Boxplots display the range from the first to the third quartile (box) and the median (centre line), while the whiskers extend to the minimum and maximum values.

https://doi.org/10.1038/s42255-025-01280-3

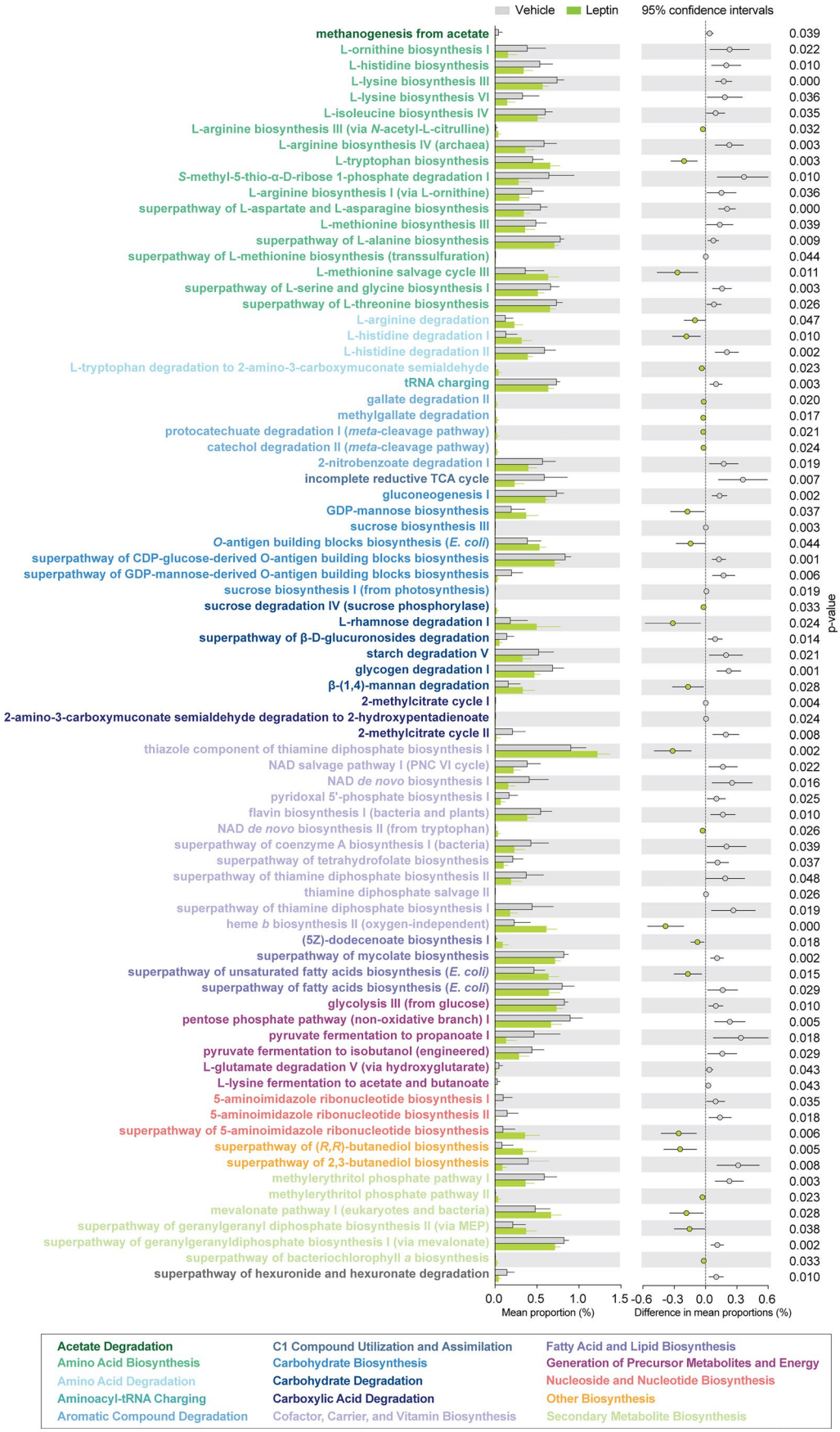

Extended Data Fig. 6 | See next page for caption.

https://doi.org/10.1038/s42255-025-01280-3

Extended Data Fig. 6 | Prediction of significantly altered functional pathways using PICRUSt2 analysis in the duodenum of leptin-treated mice. A total of 79 pathways exhibited statistically significant changes in the duodenum between vehicle-treated and leptin-treated mice at four hours post-treatment. Bar plots on the left side illustrate the mean proportion (%) of each functional pathway, while dot plots on the right side depict the differences in mean proportions (%) between the two groups (n = 8 mice per group). Statistical differences between groups were assessed using Welch's t-test, and the significance of each pathway is indicated by the corresponding p-values. Pathways are grouped according to specific functional categories, visually represented by a colour code.

https://doi.org/10.1038/s42255-025-01280-3

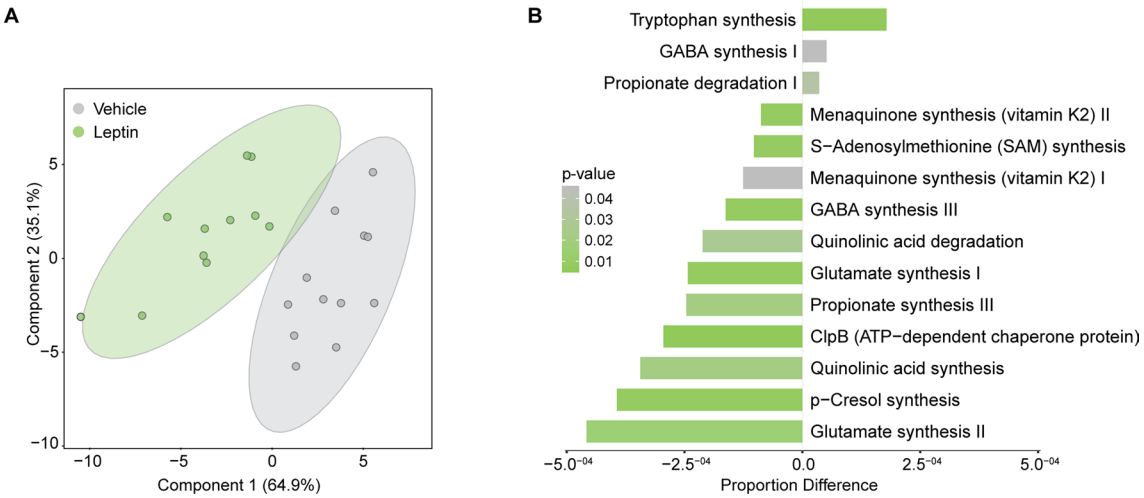

Extended Data Fig. 7 | Metabolomics and neuroactive potential analysis. **a.** Partial Least Squares Discriminant Analysis (PLS-DA) of duodenal metabolomics data showing differential clustering between vehicle- and leptin-treated groups (n = 6 mice per group). **b.** Bar plot illustrating statistically significant differences in gut-brain modules (GBMs) between leptin- and vehicle-treated groups (n = 8 mice per group). Data are presented as proportional differences, along with corresponding p-values.

nature portfolio

Corresponding author(s): patrice.cani@uclouvain.be
ruben.nogueiras@usc.es
mclaret@recerca.clinic.cat

Last updated by author(s): Feb 20, 2025

Reporting Summary

Nature Portfolio wishes to improve the reproducibility of the work that we publish. This form provides structure for consistency and transparency in reporting. For further information on Nature Portfolio policies, see our Editorial Policies and the Editorial Policy Checklist.

Statistics

For all statistical analyses, confirm that the following items are present in the figure legend, table legend, main text, or Methods section.

n/a	Confirmed	
☐	☒	The exact sample size (*n*) for each experimental group/condition, given as a discrete number and unit of measurement
☐	☒	A statement on whether measurements were taken from distinct samples or whether the same sample was measured repeatedly
☐	☒	The statistical test(s) used AND whether they are one- or two-sided *Only common tests should be described solely by name; describe more complex techniques in the Methods section.*
☒	☐	A description of all covariates tested
☐	☒	A description of any assumptions or corrections, such as tests of normality and adjustment for multiple comparisons
☐	☒	A full description of the statistical parameters including central tendency (e.g. means) or other basic estimates (e.g. regression coefficient) AND variation (e.g. standard deviation) or associated estimates of uncertainty (e.g. confidence intervals)
☐	☒	For null hypothesis testing, the test statistic (e.g. *F*, *t*, *r*) with confidence intervals, effect sizes, degrees of freedom and *P* value noted *Give P values as exact values whenever suitable.*
☒	☐	For Bayesian analysis, information on the choice of priors and Markov chain Monte Carlo settings
☒	☐	For hierarchical and complex designs, identification of the appropriate level for tests and full reporting of outcomes
☒	☐	Estimates of effect sizes (e.g. Cohen's *d*, Pearson's *r*), indicating how they were calculated

Our web collection on statistics for biologists contains articles on many of the points above.

Software and code

Policy information about availability of computer code

Data collection

Image acquisition: Nikon Eclipse Ni-U fluorescence microscope
ELISA measurements: Microplate readers, Infinite® 200 PRO (Tecan)
Blood glucose concentration: glucose meter Nova Pro Biomedical
Body weights: precision scale KERN PCB 10002
RNA quantification and integrity: Agilent 2100 Bioanalyzer (Agilent RNA 6000 Nano Kit; Agilent)
Dionex Ultimate 3000 RS LC-system coupled to an Orbitrap mass spectrometer (QExactive, ThermoFisher Scientific)

Data analysis

16S rRNA gene sequencing: FASTQ data of demultiplexed samples were downloaded from Illumina BaseSpace Sequence Hub using the BaseMount tool (v0.14 Alpha). Paired-end reads of all samples were merged using USEARCH (v11.0.667) Data analysis was performed in R (v4.4.0), using the following packages: phyloseq (v1.48.0), ANCOMBC (v2.6.0), RColorBrewer (v1.1-3), ggplot2 (3.4.4) , pheatmap (v1.0.12) and circlize (v0.4.16).
Metabolic predictions: PICRUSt2 (v2.5.2) was used to predict the metabolic signatures of the microbial communities within the QIIME2 (v.2024.2) environment. Rarefied pathway abundances were further analysed in STAMP (v2.1.3).
Neuroactive potencial: GBMs were inferred from the ortholog abundance table obtained with PICRUSt2 (v2.5.2), using the web application GOmixer (http://www.raeslab.org/gomixer/).
Metabolomics: Compound Discoverer 3.3 (ThermoFisher Scientific) was used for metabolomics data processing; mixOmics v6.28.0 and ggplot2 (3.4.4) R packages.
RNAseq analysis: Raw reads passed the quality controls established in the FastQC software (http://www.bioinformatics.babraham.ac.uk/projects/fastqc) and were mapped to the reference genome mm10 by using Hisat (v2.2.1). Further analysis was done using EdgeR (v3.42.0), limma (v3.60.4) and ggaluvial (v0.12.5) from Bioconductor (v3.19), ggfortify (v0.4.16), and ggplot2 (v3.4.4) in R (v4.4.0). Gene ontology (GO) and pathway enrichment analysis of the DEGs were performed using AmiGO 2 (https://amigo.geneontology.org/amigo).

Image analysis: ImageJ/FIJI (v2.1.0/1.53c).
Graphs and statistics analysis: GraphPad Prism (v8).

For manuscripts utilizing custom algorithms or software that are central to the research but not yet described in published literature, software must be made available to editors and reviewers. We strongly encourage code deposition in a community repository (e.g. GitHub). See the Nature Portfolio guidelines for submitting code & software for further information.

Data

Policy information about availability of data

All manuscripts must include a data availability statement. This statement should provide the following information, where applicable:

- Accession codes, unique identifiers, or web links for publicly available datasets
- A description of any restrictions on data availability
- For clinical datasets or third party data, please ensure that the statement adheres to our policy

Source data are provided with this paper. The RNA-Seq datasets generated and analysed during the study are available in the NCBI GEO repository under accession number GSE266230 (https://www.ncbi.nlm.nih.gov/geo/query/acc.cgi?acc=GSE266230). The clean reads were mapped to the reference genome GRCm38 from GCA_000001635.2 (https://www.ncbi.nlm.nih.gov/datasets/genome/GCF_000001635.20/).The metagenomic data have been deposited in the NCBI Sequence Read Archive under accession ID PRJNA1107501 (https://www.ncbi.nlm.nih.gov/bioproject/PRJNA1107501). The metabolomics data have been deposited at the Metabolomics Workbench, with project number PR002229 and accessible through http://dx.doi.org/10.21228/M8H822.

Research involving human participants, their data, or biological material

Policy information about studies with human participants or human data. See also policy information about sex, gender (identity/presentation), and sexual orientation and race, ethnicity and racism.

Reporting on sex and gender	N/A
Reporting on race, ethnicity, or other socially relevant groupings	N/A
Population characteristics	N/A
Recruitment	N/A
Ethics oversight	N/A

Note that full information on the approval of the study protocol must also be provided in the manuscript.

Field-specific reporting

Please select the one below that is the best fit for your research. If you are not sure, read the appropriate sections before making your selection.

☒ Life sciences ☐ Behavioural & social sciences ☐ Ecological, evolutionary & environmental sciences

For a reference copy of the document with all sections, see nature.com/documents/nr-reporting-summary-flat.pdf

Life sciences study design

All studies must disclose on these points even when the disclosure is negative.

Sample size	We conducted a sample size calculation using astatistical methods (https://www.datarus.eu/en/applications/granmo/) as required by the Ethical authorities. In addition, the sample size for each experiment was also aligned with our previous studies (PMID: 35108514; PMID: 38740509). All "n" values have been provided in the figure legends.
Data exclusions	For metagenomics studies, one technical outlier was identified. Its exclusion was based on the identification of a sample with total read counts below 30,000, which is a commonly accepted threshold for ensuring reliable detection of microbial taxa in sequencing data. Low read counts can result from technical issues such as insufficient sample quality or processing errors, leading to an incomplete or skewed representation of the microbial community (Supplementary Figure 1). In the other studies, data was excluded based on the ROUT test (1%) using the GraphPad Prism v8.0.
Replication	All microbiota sequencing experiments were conducted once due to the large sample size (approximately 1000 samples). To account for genetic and physiological variability, we used littermate mice from at least two different cohorts, with the experiments spaced several months apart. All other experiments were replicated at least once, with successful replication in every attempt. To ensure reproducibility, we have made all datasets publicly available and provided comprehensive details on the software, reagents, and protocols in the methods section. Individual data points were plotted, and source data is accessible. Information regarding the statistical tests used is included in the figure legends.
Randomization	Mice were randomly distributed before receiving experimental treatments.

Blinding	Data collection and analysis were not performed blind to the conditions of the experiments, except image acquisition and analysis.

Reporting for specific materials, systems and methods

We require information from authors about some types of materials, experimental systems and methods used in many studies. Here, indicate whether each material, system or method listed is relevant to your study. If you are not sure if a list item applies to your research, read the appropriate section before selecting a response.

Materials & experimental systems

n/a	Involved in the study
☐	☒ Antibodies
☒	☐ Eukaryotic cell lines
☒	☐ Palaeontology and archaeology
☐	☒ Animals and other organisms
☒	☐ Clinical data
☒	☐ Dual use research of concern
☒	☐ Plants

Methods

n/a	Involved in the study
☒	☐ ChIP-seq
☒	☐ Flow cytometry
☒	☐ MRI-based neuroimaging

Antibodies

Antibodies used	The list of all antibodies used in this study can be found in the Extended Figure 1 and Extended Figure 3 rabbit anti-FOS antibody, Synaptic Systems #226008 rabbit anti-POMC precursor antibody, Phoenix Pharmaceuticals #H-029-30 donkey anti-rabbit Alexa Fluor 647 Life Technologies #A32795 donkey anti-rabbit Alexa Fluor 488, Life Technologies #A21441 chicken anti-FOS antibody, Synaptic Systems #226009 goat anti-chicken Alexa Fluor 488, abcam #ab150169
Validation	All commercial antibodies were validated by manufactory. The validation information on their webpages are listed below: Rabbit anti-FOS antibody, Synaptic Systems #226008 https://www.sysy.com/product/226008#list Rabbit anti-POMC precursor antibody, Phoenix Pharmaceuticals #H-029-30 http://www.phoenixbiotech.net/catalog/product_info.php?products_id=6545 Donkey anti-rabbit Alexa Fluor 647 Life Technologies #A32795 https://www.thermofisher.com/antibody/product/Donkey-anti-Rabbit-IgG-H-L-Highly-Cross-Adsorbed-Secondary-Antibody-Polyclonal/A-31573 Donkey anti-rabbit Alexa Fluor 488, Life Technologies #A32790 https://www.thermofisher.com/antibody/product/Donkey-anti-Rabbit-IgG-H-L-Highly-Cross-Adsorbed-Secondary-Antibody-Polyclonal/A32790 https://www.sysy.com/product/226009#list https://www.abcam.com/en-us/products/secondary-antibodies/goat-chicken-igy-h-l-alexa-fluor-488-ab150169?srsltid=AfmBOooogXSBui1-VP3oIchiZV21peLK62kUnTi9n6qVTD0aSVTcn-68

Animals and other research organisms

Policy information about studies involving animals; ARRIVE guidelines recommended for reporting animal research, and Sex and Gender in Research

Laboratory animals	Mice were group housed (4–5 animals per cage) under controlled environment regarding relative humidity (30%-80%) and temperature (20–24°C), in a 12-hour light/dark cycle and allowed to freely access water and standard diet (Teklad maintenance diet 14% protein; Envigo). In particular studies, the high-fat diet (60% Kcal from fat, 4.7 kcal/g; Research Diets) was provided ad libitum for twelve weeks (starting at six weeks of age). C57BL/6J, POMCcre/+ and AgRPcre/+ mice were bred in-house. As controls, Cre-negative littermates were used.
Wild animals	The study did not involve wild animals.
Reporting on sex	Sex was not considered in this study.
Field-collected samples	The study did not include samples collected from the field.
Ethics oversight	All animal studies adhered to the ethical standards approved by the Ethics Committee of the University of Barcelona (390/19) and the University of Santiago de Compostela (15012/2023/014) in accordance with current local, national, and European legislation.

Note that full information on the approval of the study protocol must also be provided in the manuscript.

Plants

Seed stocks

Report on the source of all seed stocks or other plant material used. If applicable, state the seed stock centre and catalogue number. If plant specimens were collected from the field, describe the collection location, date and sampling procedures.

Novel plant genotypes

Describe the methods by which all novel plant genotypes were produced. This includes those generated by transgenic approaches, gene editing, chemical/radiation-based mutagenesis and hybridization. For transgenic lines, describe the transformation method, the number of independent lines analyzed and the generation upon which experiments were performed. For gene-edited lines, describe the editor used, the endogenous sequence targeted for editing, the targeting guide RNA sequence (if applicable) and how the editor was applied.

Authentication

Describe any authentication procedures for each seed stock used or novel genotype generated. Describe any experiments used to assess the effect of a mutation and, where applicable, how potential secondary effects (e.g. second site T-DNA insertions, mosiacism, off-target gene editing) were examined.